



Nanoscale

Topology of Transition Metal Dichalcogenides: The Case of the Core-Shell Architecture

Journal:	<i>Nanoscale</i>
Manuscript ID	NR-REV-09-2020-006660.R1
Article Type:	Review Article
Date Submitted by the Author:	16-Nov-2020
Complete List of Authors:	DiStefano, Jennifer; Northwestern University Murthy, Akshay; Northwestern University Hao, Shiqiang; Northwestern University, dos Reis, Roberto; Northwestern University, Materials Science and Engineering Wolverton, Chris; Northwestern University, Department of Materials Science and Engineering Dravid, Vinayak; Northwestern University, Materials Science & Engineering

SCHOLARONE™
Manuscripts

Topology of Transition Metal Dichalcogenides: The Case of the Core-Shell Architecture

Jennifer G. DiStefano ^{a,c}, Akshay A. Murthy ^{a,c}, Shiqiang Hao ^a, Roberto dos Reis ^{a,b}, Chris Wolverton ^a,
Vinayak P. Dravid ^{a,b,c}

^a Department of Materials Science and Engineering, ^b Northwestern University Atomic and Nanoscale Characterization Experimental (**NUANCE**) Center, and ^c International Institute for Nanotechnology (IIN), Northwestern University, Evanston, Illinois 60208, USA

* Corresponding Author: v-dravid@northwestern.edu

Abstract

Non-planar architectures of the traditionally flat 2D materials are emerging as an intriguing paradigm to realize nascent properties within the family of transition metal dichalcogenides (TMDs). These non-planar forms encompass a diversity of curvatures, morphologies, and overall 3D architectures that exhibit unusual characteristics across the hierarchy of length-scales. Topology offers an integrated and unified approach to describe, harness, and eventually tailor non-planar architectures through both local and higher order geometry. Topological design of layered materials intrinsically invokes elements highly relevant to property manipulation in TMDs, such as the origin of strain and its accommodation by defects and interfaces, which have broad implications for improved material design.

In this review, we discuss the importance and impact of geometry on the structure and properties of TMDs. We present a generalized geometric framework to classify and relate the diversity of possible non-planar TMD forms. We then examine the nature of curvature in the emerging core-shell architecture, which has attracted high interest due to its versatility and design potential. We consider the local structure of curved TMDs, including defect formation, strain, and crystal growth dynamics, and factors affecting the morphology of core-shell structures, such as synthesis conditions and substrate morphology. We conclude by discussing unique aspects of TMD architectures that can be leveraged to engineer targeted, exotic properties and detail how advanced characterization tools enable detection of these features. Varying the topology of nanomaterials has long served as a potent methodology to engineer unusual and exotic properties, and the time is ripe to apply topological design principles to TMDs to drive future nanotechnology innovation.

Introduction

Much of the elegance of materials science is captured by the classic structure-processing-property-performance paradigm which encompasses key design principles for accessing novel materials. Traditionally, structure referred to understanding and engineering microstructure and nanostructure without express emphasis on global geometry. Topology – the way in which physical shape or geometry impacts material properties – serves as another important component of the structure pillar, particularly for nanomaterials.^{1,2} Indeed, materials scientists have employed aspects of topological design throughout the history of nanotechnology to produce exotic properties. Spatial confinement, often realized through unique architectures, is well known for inducing unusual material properties for electronic, optical, biomedical, and energy applications. For instance, curvature has enabled important technological innovation in organic and inorganic materials alike, including quantum dots³, carbon nanostructures^{4,5}, and III-V semiconductors⁶. Carbon nanostructures have received particular interest due to their ability to form countless geometries and their associated new physics.^{7,8} The many allotropes of sp^2 carbon, ranging from fullerenes to pillared graphene, provide a glimpse into the numerous geometries possible with other nanomaterial systems.⁹

As the semiconducting analog of carbon nanostructures, transition metal dichalcogenides (TMDs) provide a rich platform for topological design. TMDs are particularly ripe to be curved, bent, stretched, and twisted due to their ability to accommodate significant strain.¹⁰ This mechanical compliance and strain tolerance enable TMDs to adopt numerous geometries. Indeed, a broad array of unique TMD architectures have been demonstrated such as scrolls^{11–13}, 3D spirals^{14–17}, hollow spheres¹⁸, toroids¹⁹, quantum dots²⁰, open and closed nanotubes^{21,22}, nanooctahedra^{23,24}, and nanoboxes^{25–27}. Moreover, unique opportunities emerge within curved TMDs to further tune chemical, electronic, and optical properties. For instance, strain engineering is a powerful method for modulating optical^{28,29} and phonon^{30,31} bandgaps. Geometries with highly localized strain are particularly useful for funneling

excitons³² and single-photon emission^{30,31}. While many geometric varieties of TMDs exist in isolated reports, a unified framework and discussion of topology in TMDs remains lacking.

Here, we consider the application of this architectural strategy to TMDs and aim to further establish topology as an approach to induce unique material properties. We first introduce a topological classification system specific to layered materials to relate complex geometries to the familiar planar TMD structure. This framework is intended to not only identify gaps in current geometries but also to serve as a living platform to be continuously expanded as new geometries are identified. We then focus on the core-shell architecture and examine the role of curvature in this templated structure. We leverage prior work on curved layered materials – both carbon nanostructures and TMDs – to examine the structure of the TMD shells. We connect current literature, fundamental theory, and original experimental and theoretical results to discuss defect formation and nanoscale structure. We conclude by discussing some of the numerous emerging opportunities to further probe and design TMD core-shell architectures using topology.

I. Architecture in 2D Materials

Non-planar TMDs include any structures that exist beyond a single plane, such as wrinkled monolayers, spherical fullerenes, and closed and open nanotubes. However, there is a critical topological distinction within the general category of “non-planar” structures. Some non-planar structures, such as open nanotubes and wrinkled monolayers, can be directly manipulated into a planar TMD without stretching, tearing, or gluing and therefore with no change in atomic arrangement. Others, however, fundamentally cannot be deformed into a planar TMD, such as a sphere or closed nanotube, without rearranging atomic bonding. Therefore, two distinct categories emerge – those geometries which are deformed planar TMDs and those which are impossible to flatten into planar sheets. This distinction is at the heart of topological design of curved TMDs and can be understood by considering the definition of Gaussian curvature.

Gaussian curvature is defined as the product of the two principle curvatures of a surface.¹ As such, there are three possible types of geometries for a surface in 3D space: (i) zero Gaussian curvature, where at least one principle curvature is zero; (ii) positive Gaussian curvature, where the two principle curvatures have the same sign, such as in a spheres and ellipsoids; and (iii) negative Gaussian curvature, where the principle curvatures have opposite signs, such as in a saddle point or hyperbolic shape.⁸ Importantly, bending a surface without stretching it does not change the type of Gaussian curvature.³³ For instance, a planar graphene layer rolled into a nanotube exhibits zero Gaussian curvature just like the planar parent layer. This can be understood by considering that an open-ended nanotube is only curved in one dimension and therefore the product of its principle curvatures remains zero. However, a nanotube with closed, rounded ends exhibits principle curvatures in the same direction on the endcaps, making it a positively curved nanostructure. Accordingly, a closed nanotube cannot be deformed into a planar sheet and therefore is not topologically equivalent to the open-ended nanotube. This example demonstrates the important concept that zero Gaussian curvature includes but is not limited to planar structures. Many non-planar geometries also do not, by definition, exhibit Gaussian curvature. Curved structures are inherently non-planar and cannot be deformed into a zero curvature structure because, as will be discussed at length, they possess that curvature due to built-in topological defects. As such, curved structures exhibit atomic arrangements, and therefore properties, distinct from non-planar zero curvature structures. Although other definitions of curvature exist, we reference the definition of Gaussian curvature in the remainder of this text when discussing curved TMDs.

Materials scientists often categorize structures using dimensionality and are familiar with the progression from a planar 1D carbon nanoribbon to 3D graphite. After all, dimensionality is inherent to the nomenclature describing the field of 2D materials itself. However, further classifying nanostructures, and particularly those based on layered materials, has posed an ongoing challenge.⁹ Indeed, not all carbon and TMD nanostructures can be directly related using dimensionality alone, in part due to the sometimes

arbitrary dimensionality definitions applied to complex nanostructures. For instance, both a planar MoS₂ quantum dot and spherical MoS₂ inorganic fullerene are typically classified as 0D structures, even though a fullerene protrudes into a third dimension that a quantum dot does not. Further, a helical nanotube might be considered 1D, since it extends primarily in a single direction; however, a straight nanotube is also classified as 1D and clearly these two structures exhibit different dimensionality. As a result, more complex architectures are excluded from the traditional dimensionality framework designed for planar layered materials. It is therefore insufficient to classify carbon and TMD nanostructures solely based on dimensionality to capture the full picture of topological diversity and opportunity.

We propose that the missing parameter in this context is curvature and present a framework that combines curvature with dimensionality (Figure 1). This framework is intended to elucidate relationships between nanostructures that are not fully captured using a simple dimensionality approach and assist researchers in methodically relating newly discovered nanostructures to existing ones. Our categorization and use of “architecture” throughout this work focuses on individual exotic nanostructures (e.g. carbon nanopyrramids³⁴) – either periodic or stand-alone – rather than hierarchical assemblies or hybrid nanostructures (e.g. graphene-nanotube hybrids³⁵). Categorization of nanostructure assemblies has been detailed previously^{36,37} and could be utilized in concert with our proposed framework.

We present this classification scheme for nanostructures which are experimentally demonstrated or calculated derivatives of layered materials. Several design elements and constraints are key to interpreting the geometric framework for a given layered compound:

1. We define 0D nanostructures as the simplest (either most symmetrical or fewest atoms) examples within a given curvature category. In other words, they serve as the best approximation for a point object for a given curvature.
2. Along a given curvature pathway, the 0D structure is extended (i.e. repeated) in a single direction to produce the 1D structure.

3. The 1D structure is either bent or extended orthogonally to produce the 2D structure. Continuous surfaces are formed when necessary.
4. 1D and 2D structures are defined as those that do not exceed the out-of-plane dimension of the 0D structure.
5. The 2D structure is bent or extended in the third dimension to produce the 3D structure.
6. Mixed curvature is defined as a combination of positive and negative curvature.
7. Each structure must represent the appropriate curvature. For instance, an open nanotube could be distorted to form a torus but doing so would change the curvature from zero (for the nanotube) to mixed (for the torus) and thus is forbidden along the zero curvature pathway.

Additionally, many nanostructures are known to possess local positive and negative curvature as dictated by the local atomic arrangement.³⁸ Here, we focus on the global curvature of the entire structure and apply the assumption that global curvature is representative of local atomic arrangement, but the nuances of curvature in nanostructures should be noted and recognized as often more complex.

We begin by examining the traditional progression of dimensionality involving planar structures. The 0D building block for a planar layered material is a monolayer quantum dot. Following the prescribed operations, the quantum dot is extended in 1D to form a nanoribbon, which is extended in the orthogonal direction to form a 2D monolayer. Notably, the nanoribbon is not extended vertically since that operation would violate rule 4. Finally, the monolayer is repeated vertically to form a multilayer structure. The non-planar pathway demonstrates the possibility of maintaining zero Gaussian curvature and forming only non-planar structures. However, it also demonstrates how more complex curved structures are related to those structures with zero curvature. A 1D open nanotube can be repeated and formed into a continuous surface to produce a wrinkled sheet, thus staying within the confines of the non-planar definition. However, it can also bend to form a torus, which is known to possess positive curvature on the outer surface and negative on the inner surface.^{39,40} Therefore, a separate pathway branches off for mixed

curvature. The 2D wrinkled sheet and torus are then bent and extended out-of-plane, respectively, to form 3D structures.

Positive and negative curvature each introduce gaps in the geometric framework. To progress from a closed nanotube to 2D, the nanotube must be repeated or extended in the orthogonal direction (bending would induce negative curvature and thus is forbidden⁴⁰). A possible resulting nanostructure is a thin “nanopocket” with height analogous to the nanotube; however, no such structures have yet been demonstrated. Extending the hypothetical nanopocket vertically produces a non-spherical closed, positively curved 3D structure. Nanooctahedra therefore represent a potential positive 3D structure and have been composed of a wide variety of TMDs.⁴¹ The basic structure demonstrating only negative curvature has been previously proposed as a catenoid⁴²; however, 1D analogs are lacking. Much work has been done on the 2D analog of carbon nanotube networks⁴³ (also called pillared graphene) and the duplication into 3D to create periodic carbon schwartzites.⁴⁴ Notably, the planar zero curvature progression in dimensionality is the only case where the 0D, 1D, and 2D structures can be fabricated directly from the 3D structure. In each of the others, changes in bonding are required to move from one dimensionality to another and the ability to fabricate each structure from the 3D analog does not necessarily hold for curved structures. We intend this figure to serve as a demonstration of this powerful approach of combining curvature and dimensionality and challenge the community to continue to populate this framework with additional nanostructures. There is ample opportunity to adapt this framework for complex structures, such as branching into different curvatures from a common structure, of which we have demonstrated an example.

A critical distinction among the structures presented in this geometric framework arises between hollow nanostructures (e.g. inorganic fullerenes and nanorods) and those constructed on templates (e.g. core-shell structures, schwartzites). There have been numerous reports reviewing investigations of synthesis, theoretical modeling, and applications of hollow inorganic nanostructures, which are being

explored for an array of attractive opportunities.⁴⁵⁻⁵¹ For instance, curvature-induced defects and plentiful edge sites in TMD inorganic fullerenes increase catalytic activity for hydrogen evolution reaction (HER).^{52,53} Inorganic fullerenes are further being investigated for their superior tribological behavior⁴⁹ and as high performance battery materials.⁵¹ The reduction in crystal symmetry in inorganic nanotubes can be leveraged for photovoltaic effects.⁵⁴ A recent report noted that hybridized core-shell structures demonstrate particular promise for renewable energy applications compared to hollow nanostructures alone.⁴⁹

Templated substrates have been less studied than their hollow counterparts but present a method to create complex TMD geometries, such as carbon schwarzites, that can otherwise be quite challenging to synthesize.⁴⁴ Specifically, templates are one strategy that could be employed to design new architectures to fill in the gaps in this framework and explore alternate pathways. Further, templates can enable unprecedented control of crystal structure and material properties in curved layered materials. Enhanced synthetic control over curved TMDs is a prerequisite to achieving nanoscale structure control, and this can be enabled by structurally complex template materials. Thus, templated curved layered materials provide an intriguing platform to build the next generation of curved layered materials with exquisite structure and property control. The remainder of this work will consider one such templated structure – a rigid nanoparticle core encapsulated by a TMD to form a core-shell structure. Although our focus is on the curved core-shell architecture, hollow nanostructures remain critical to inform our understanding of this system.

II. The TMD Core-shell Architecture

Within this broader portfolio of curved TMDs, the TMD core-shell architecture, with the common notation core@shell, offers unique functionality that makes it promising for targeted applications and property manipulation. For example, TMD core-shells offer the inherent opportunity to hybridize TMDs

with functional core nanomaterials to tailor properties and produce synergistic effects. The core-shell structure maximizes the interfacial area between the core and shell nanomaterials, unlike a flat TMD film which can only achieve a single point of contact with a spherical nanoparticle. Further, creating and strategically positioning defects in TMDs offers a useful method for property engineering and one that is intrinsically accessible in the core-shell architecture by modulating curvature. The core-shell structure also provides a natural platform to leverage built-in strain to tune electronic and chemical properties. Both local and global strain could be purposefully designed via the core dimensions to induce exciton funneling or alter chemical reactivity with a target molecule. Finally, TMD core-shells can serve as building blocks of complex hierarchical structures with exotic properties, either through direct assembly of core-shells or shells composed of multiple TMDs within a single core-shell structure.⁵⁵

The structure-processing relationship is particularly critical for non-equilibrium curved structures, which we will explore in depth. However, it is first useful to briefly review the various methods used to prepare TMD core-shells, including both vapor-phase and solution-based approaches. In most cases, the nanoparticle cores are prepared prior to TMD encapsulation. Controllable synthetic routes, such as chemical vapor deposition^{56,57} and thermolysis⁵⁵, designed for planar TMDs can be easily adopted to produce highly crystalline, curved TMDs through the use of nanoparticle cores, presenting a key advantage of templated growth. Additionally, solvothermal methods^{58,59} can be preferable for solution-based applications or in situations where an increased density of defects is advantageous. Modification of core-shells can be employed for further engineering through methods such as core removal¹⁸ to create hollow TMD shells and metal deposition on TMD shells for additional hybridization.⁶⁰

Leveraging synergistic effects between the core and TMD shell to produce interesting electronic and optical properties has been a fruitful research area in recent years. Plasmonic nanoparticle cores have been leveraged to enhance photoluminescence of TMD shells^{56,57} and form plasmonic hot spots.⁶⁰ Based on these properties, several optoelectronic devices utilizing core-shells have been demonstrated with

superior performance to their planar counterparts.^{18,61} TMD shells can also be constructed on templates of other layered materials, such as carbon nanotubes and nanospheres.^{62,63} Carbon nanotube@TMD structures demonstrate strong promise in energy storage devices, attributed in part to the high TMD interlayer spacing facilitating ion diffusion.^{64–68} Several studies demonstrate the potential of TMD core-shell structures for hydrogen production,⁶⁹ particularly when hybridization is combined with controlled defect formation through unusual core shapes^{70,71} or vertical growth⁷². Additionally, TMD core-shells have shown promise in sensing applications, such as gas sensing⁷³ and SERS^{58,59}, and biomedical applications including glucose detection⁷⁴ and photothermal therapy⁷⁵.

The majority of work on TMD core-shells to date has focused on hybridization to induce interesting properties, but ample opportunity exists to enhance and access new properties by employing the curvature inherent to these structures. Leveraging topological design, such as through curvature-induced defects and strain, would greatly expand the versatility and application potential of the core-shell paradigm. However, an in-depth understanding of the structural characteristics of curved TMDs is a prerequisite to achieving deterministic control of atomic structure. In this work, we analyze positive curvature in TMDs specifically due to its application to the core-shell structure. However, a similar analysis could be undertaken for other curved and non-planar TMD geometries. We aim to apply the existing understanding of structure of non-planar and curved TMDs to the core-shell architecture to identify important knowledge gaps and drive future research.

III. Local Core-Shell Structure

Before discussing local structural changes that arise due to curvature, we introduce the structure of a pristine TMD crystal. In a TMD monolayer, the transition metal atoms (M) are covalently bonded to two adjacent layers of chalcogen (X) atoms to form a X-M-X layer. In this review, we focus on the hexagonal 2H structural polytype, which has trigonal prismatic coordination, because of the abundant property engineering opportunities with this semiconducting phase. Importantly, hexagons do not

contribute to curvature of a surface.⁸ Hexagons can be tiled to form a 2D plane, such as a monolayer TMD layer, but it is geometrically impossible for a hexagonal lattice to form a curved surface without introducing topological defects, or ring types other than hexagons.⁷⁶ Therefore, topological defects are geometrically necessary in curved TMDs. In this section, we discuss the proposed topological defects that form curvature, the role of strain, non-topological defects, and the balance between defects and strain in curved TMDs. Limited data exist about atomic structure specific to TMD core-shells, so instead we examine defects and strain in hollow curved TMDs structures, namely inorganic fullerenes and nanotubes, with the hope of elucidating the local structure of curved TMDs in the core-shell architecture.

Topological Defects in Curved TMDs

The atomic arrangement of curved TMDs is driven by both geometric constraints and chemical interactions. Carbon nanostructures provide a simplified system to isolate the geometric constraints of curving a hexagonal lattice and understand the mathematical description of geometrically necessary defects. In the most stable configurations for curved carbon nanostructures, pentagonal rings form positive curvature and heptagonal rings form negative curvature.^{77,78} However, other topological defects can also induce positive and negative curvature. For instance, octagons can replace hexagons to induce negative curvature with minimal additional strain.⁷⁸ The relationship between defects and topology in a closed orientable surface with hexagonal structure was formalized as:

$$2N_4 + N_5 - N_7 - 2N_8 = 12(1 - g), \quad \text{Eq. 1}$$

where N_4 , N_5 , N_7 and N_8 are the number of square, pentagonal, heptagonal, and octagonal rings of carbon, respectively, and g is the genus of the structure (e.g. the number of handles or holes).⁸ Mathematically, squares and pentagons induce positive curvature while heptagons and octagons induce negative curvature. For instance, a C_{60} fullerene is a positively curved surface with a genus of 0. Based on Eq. 1, C_{60} must possess a majority of 4- and 5-member rings (in addition to hexagons) to possess that positive curvature. Similarly, a torus has a genus of 1 and, as previously discussed, contains both positive and

negative curvature. Accordingly, Eq. 1 necessitates a balance of 4- or 5-member rings with 7- or 8-member rings.

Carbon nanostructures contain a single element and thus the formation of topological defects under curvature is dictated largely by geometric constraints; however, chemical bonding between elements in multielemental compounds, such as TMDs, cause a divergence from carbon chemistry. In TMDs, it is energetically favorable to maintain stoichiometry and avoid high energy bonds (i.e. Mo-Mo or S-S), which would inevitably form in pentagonal or heptagonal rings. The suggestion that square-like topological defects, which preserve stoichiometry, create positive curvature in TMDs was first proposed in 1993.⁷⁹ This hypothesis has since been corroborated by several others via theoretical calculations and scanning/transmission electron microscopy (S/TEM) who also assert that octagonal-like defects create negative curvature in TMDs.^{23,80–82} Figure 3 demonstrates the differing topological defects needed to produce positive and negative curvature in carbon and TMD nanostructures, despite their similar pristine hexagonal structure. Further, Eq. 1 shows that square and octagonal defects contribute more to curvature than pentagonal and heptagonal defects (i.e. the factor of 2). This sharp localized curvature could lead to the appearance of faceting, which might explain why faceting occurs in inorganic fullerenes (e.g. MoS₂ and BN) at sizes where the equivalent carbon structures are spherical.⁸¹

Strain in Curved TMDs

Strain in curved TMDs can be quite complex due to the varying strain state across the thickness of the shell. A TMD sphere will experience tensile strain on the outer surface and compressive strain on the inner, altering the spacing of S-S atoms in a given layer.⁸³ Therefore, strain due to bending in 1D provides a useful reference to understand strain in 3D in TMD core-shells. The strain energy per atom (

$\frac{E_{strain}}{N}$) in a nanotube of radius R follows a $\frac{1}{R^2}$ relationship,^{80,84} with the full equation⁸⁴

$$\frac{E_{strain}}{N} = \frac{Yh^3}{24\rho_a R^2} \quad \text{Eq. 2}$$

where Y is elastic modulus, h is layer thickness, and ρ_a is the number of atoms on the surface unity of the monolayer. It is apparent from Eq. 2 that strain energy is also highly dependent on layer thickness (h) in addition to radius. It is important to note that Eq. 2 is derived from continuum mechanics and does not consider the atomic structure, including defects, of a nanotube. Strain energy in MoS_2 nanotubes is over an order of magnitude larger than that of carbon nanotubes of comparable size because of the greater thickness of an MoS_2 monolayer and the steric hinderance produced as sulfur atoms on the inside of the tube are compressed.⁸⁴ However, MoS_2 nanotubes as small as 2 nm in diameter have been observed, suggesting that the strain energy is reduced enough to form stable curved structures above this threshold.⁸⁰ The strain energy per atom of a single-shell spherical nanoparticle can similarly be derived, but the assumption of zero defects becomes problematic due to the necessary presence of topological defects in closed TMDs. However, if the number of topological defects is considered negligible compared to the total number of atoms, the strain energy per atom can be approximated as ⁸⁴

$$\frac{E_{strain}}{N} = \frac{Yh^3(1 + \sigma)}{12\rho_a R^2} \quad \text{Eq. 3}$$

where σ is Poisson's ratio. Notably, the key difference between Eq. 2 and Eq. 3 is the factor of $2(1+\sigma)$, which is necessarily positive, and indicates the higher strain energy per atom in spherical particles than nanotubes of a similar size. As will be discussed below, this increased strain energy increases the probability of defect formation in spherical TMD particles compared to nanotubes. The strain energy of multi-layered inorganic fullerenes, or "onion-like" TMD spherical structures, includes additional factors, though stability does increase with an increasing number of shells due to attractive van der Waals forces.⁸⁴ Indeed, ongoing efforts to identify single-walled inorganic fullerenes have not yet succeeded and indicate that such structures are likely unstable, which is attributed to high strain.^{23,85} Instead, multiwall inorganic fullerenes or planar nanoplatelets tend to form, depending on the number of atoms and shells.²³ Notably, core nanoparticle templates provide a route to achieve inorganic single-walled structures, as multiple demonstrations of single-shell TMD core-shell structures have been reported.^{18,86}

Energetics of Curved TMDs: Balancing Defects and Strain

There are three main components to energy of nested inorganic fullerenes: curvature elastic energy, defect energy, and surface energy.⁸⁷ Here, we discuss the competition between the elastic and defect energies; however, it should be noted that the following discussion involves strain-induced defects which include defects beyond topological defects. Topological defects must be present in curved TMDs to form the curved surface.⁸⁷ Non-topological defects, such as those presented in Figure 4, can additionally be induced by the high strain environment often present in curved TMDs.

The balance between strain energy and defect formation energy is dependent on both the radius of curvature and material thickness and can be understood by considering epitaxial thin film growth. In traditional thin film growth models, the elastic strain energy is dependent on film thickness and lattice mismatch with the substrate. Given a fixed lattice mismatch, the film thickness dictates whether the strain energy surpasses that of defect formation. Thus, critical thickness refers to the thickness above which defects form in a thin film and below which a defect-free, strained interface is predicted to form. Alternatively, for a fixed film thickness, critical lattice mismatch could be defined as the mismatch beyond which defects form in the thin film due to high epitaxial strain. In curved thin films, a similar relationship can be constructed between curvature and strain, where curvature is defined as the inverse of radius. Assuming a constant material thickness, the curvature at which strain energy exceeds defect formation energy is defined as the critical curvature.⁸⁷ Similarly, for a fixed curvature, one can determine the critical thickness above which defects form.

This theory can be applied to curved TMDs to understand the emergence of strain-induced defects. Generally, thin nested inorganic fullerenes are approximately spherical while thick nested fullerenes exhibit facets due to dislocations or grain boundary relaxation.⁸⁷ This observation is consistent with the relationship between critical curvature (κ_c) and material thickness (h) in anisotropic materials (e.g. TMDs),⁸⁸

$$\kappa_c \propto \frac{1}{h^2} \ln(h). \quad \text{Eq. 4}$$

An elastically curved film has an equilibrium dislocation density of zero for large radii and a nonzero dislocation density once the radius of curvature decreases past the critical value.⁸⁸ Similarly, this relationship manifests in curved TMDs as faceted nanooctahedra transition to semi-spherical inorganic fullerenes with increasing radius, which is readily apparent using S/TEM imaging.⁸⁷ A limited number of atoms in the nanooctahedra forces the closed structure to a small size, increasing the strain and inducing defect – and thus facet – formation. The quasi-spherical inorganic fullerene becomes stable typically at diameters greater than 30 nm and with $>10^5$ atoms.⁸²

Understanding the probability that non-topological defects, such as atomic vacancies and substitutions, will form in curved TMDs with various radii is a prerequisite to utilizing built-in defects in TMD core-shells. We evaluate the impact of curvature on non-topological defect formation energy using density functional theory (DFT) energy calculations to elucidate the most favorable defects in curved structures (Figure 4a, b). For simplicity and to explore this point further, we look at the defect formation energies in stoichiometric MoS₂ nanotubes, a model system exhibiting curvature in only one direction. Multiple studies demonstrate the impact of common point defects on the electronic and mechanical properties of TMD nanotubes, suggesting strong potential for defect engineering, and limited reports examine the formation energies of some point defects.^{89–93} We aim to supplement this work by systematically calculating the formation energies associated with these and other common defects in planar and nanotube MoS₂ geometries. We consider sulfur vacancies, sulfur divacancies, Mo vacancies, and antisite defects (Mo_S). For the sulfur vacancies, we calculate vacancies both on the inner and outer surfaces of the nanotube to assess how the different strain environments affect defect formation energy.

Figure 4b shows that, except for the outer sulfur vacancy, all non-topological defects considered are more favorable in the nanotubes than in planar layers, consistent with previous findings.⁸⁹ The nanotube geometry notably decreases the defect formation energy for some defects, such as the

difference of >6 eV between planar and nanotube structures in the case of the antisite defect. The formation energy of the outer sulfur vacancy in nanotubes closely matches that of the planar sulfur vacancy. Interestingly, the antisite defect and sulfur divacancy each exhibit a slight increase in formation energy with increasing nanotube diameter, while the other defects show no clear dependence on size. These results show that, of the most common point defects in TMDs, antisite defects and inner sulfur vacancies and divacancies are the most favorable defects to form under extreme curvature. Additionally, defect formation can potentially be controlled by varying the curvature, which could provide a pathway for targeted defect engineering in curved TMDs.

Examining the atomic structure of other curved TMDs provides important insight into that of TMD core-shells. However, it is worth noting that the fixed radius in the core-shell geometry complicates the energetics of the system compared to self-assembled, hollow curved nanostructures (e.g. inorganic fullerenes and nanotubes). The curved TMD in a core-shell geometry cannot fully relax and is instead limited to the fixed radius of the nanoparticle core with a fixed number of atoms composing the shell. Experimental and theoretical investigations detailing the thickness, radius, and core material combinations that induce faceting, and thus surpass the critical thickness of TMD shells, could elucidate how the energetics of TMD core-shells differ from those of hollow curved TMDs. Additional experimental reports⁹⁴ that examine TMD growth on curved substrates could also inform this relationship and facilitate defect engineering in TMD core-shells. While the templated substrate, and resultant fixed radius, in the core-shell architecture complicates the system energetics, it also provides a controllable and powerful method to engineer strain and defects into TMDs.

IV. Global Core-Shell Structure

In addition to local structure, it is important to consider nanoscale or global structure of TMD core-shells which can impart further design opportunities. Tuning morphology serves as a powerful route for controlling electronic, optical, and particularly chemical properties in TMDs, such as by modulating

attachment sites for molecules. Indeed, maximizing active sites of TMD crystals for hydrogen binding has been an area of intense interest in recent years.^{95–99} TMD core-shells are particularly ripe for morphological engineering because they present a variety of parameters that can dictate the resultant global structure. The following section highlights three major contributions to global structure and morphology in TMD core-shells: (1) the interface energies of the system; (2) the synthesis conditions; and (3) the morphology of the core material. A core-shell morphology pathway schematic (Figure 5) summarizes the key factors affecting shell morphology discussed in this section.

Formation of complete shell in vapor-based synthesis

The first aspect of global core-shell structure we consider is the formation of a complete TMD shell in CVD. In this synthesis process, bare nanoparticle cores sit on a flat substrate while the TMD is deposited from vapor phase. Therefore, one might expect a gap in the TMD shell where the core is in contact with the substrate. However, overwhelming experimental evidence, including cross-sectional TEM analyses, has shown that fully encapsulated nanoparticles result from this process.^{18,56,57,100} An analysis of the energetics of the system helps to explain the growth dynamics of this full encapsulation. We first consider the energy cost of the TMD shell/nanoparticle core interface formation. Previously, chemical bonding between the core and shell materials was hypothesized to be a prerequisite for conformal TMD encapsulation, largely based on the successful demonstration of Au@MoS₂ and the well-established gold-sulfur bonding affinity.¹⁰¹ However, our subsequent analysis elucidated that the core/shell interface formation energy, rather than chemical bonding specifically, dictated encapsulation.⁵⁶

To complete our understanding of the formation of a TMD shell, we must consider not only the thermodynamic driving forces of nucleation related to the core/shell interface but also the shell/substrate and core/substrate interfaces. In a recent report, we investigated the synthesis of Au@MoS₂ on an SiO₂/Si substrate.¹⁰⁰ DFT theoretical calculations revealed that the Au(111) and SiO₂ surfaces are thermodynamically favorable surfaces for MoS₂ deposition and that the Au/SiO₂ exposed interface is the

highest energy. Therefore, the Au/SiO₂ interface is expected to be the most active site for MoS₂ nucleation. Once nucleated, the MoS₂ continues to grow along the Au/SiO₂ interface beneath the Au nanoparticle as well as along the exposed Au surface. Thus, complete encapsulation is achieved. This can be understood not only in terms of minimizing the interface energy of the system but also by considering the driving force to minimize edges of TMD layers. Due to anisotropic bonding in TMD layers, elimination of dangling bonds through closed structures, like shells, minimizes surface energy.¹⁰²

This energy minimization scenario is of course highly dependent on the core, shell, and substrate materials and their interactions; however, it provides insight into the relative material requirements for the formation of complete TMD shells. Based on this analysis, the relative thermodynamic favorability of the possible growth surfaces within a system can be used to predict the probability of achieving a complete, conformal encapsulation, which is the first decision node in Figure 5. Figure 4c provides DFT interface formation energy calculation results for MoS₂ and several core materials. These data suggest it is feasible to encapsulate Si and Cu cores using a similar process to Au core encapsulation since their interface formation energies with MoS₂ are comparable.

Effect of synthesis conditions on TMD nanoscale morphology

Several morphologies of TMD core-shells have been documented in literature beyond the conformal shell, such as winged and flower-like shells.^{72,103,104} These alternate morphologies can typically be controlled by manipulating the synthesis conditions to create kinetically trapped structures. In a previous study, we found that placing the sulfur precursor in a higher temperature region of the furnace led to a “winged” core-shell morphology, where TMD layers extend from the core.⁵⁶ Further, increased growth time under these conditions results in the continued growth of these wings and the formation of a flower-like core-shell structure.⁷² Interestingly, the sulfur evaporation rate is a common lever across TMD CVD literature used to alter nucleation rate and growth speed to create unusual morphologies. Fast sulfur evaporation reportedly leads to supersaturated MoS₂ vapor and creates an excess of nucleation

sites, resulting in vertically aligned MoS₂ layers.¹⁰⁵ Similarly, CVD MoSe₂ vertical layers have been grown using a seeding promoter to increase nucleation sites and growth speed.¹⁰⁶ Another study reports MoS₂ helical spirals synthesized by quickly evaporating sulfur, supersaturating the sulfur vapor pressure and causing a higher partial pressure of MoO_{3-x} which increases the nucleation rate.¹⁵ The nucleation rate is expected to increase dramatically beyond a critical supersaturation point of sulfur.¹⁴ Accordingly, traditional planar growth is observed in this study at a low sulfur evaporation rate. Further, rapid sulfurization or selenization of a transition metal (Mo, W) creates a kinetically controlled growth environment limited by the sulfur diffusion rate, producing vertically aligned layers.^{102,107,108} Although these growth dynamics are not directly comparable to those in CVD, they do provide further evidence of alternate TMD morphologies forming when a system is pushed away from equilibrium. These findings support the hypothesis that increased sulfur vapor pressure induces rapid impingement of precursors that increases the nucleation rate and forms the winged and flower-like morphologies of TMD core-shells. The morphology pathway schematic (Figure 5) reflects that growth conditions far from equilibrium induce winged or flower-like morphologies, depending on the growth time.

Effect of growth surface on TMD nanoscale morphology

A final variable affecting the global structure of TMD core-shells is the morphology of the core nanoparticle itself. As previously discussed, the interfacial energy between core and shell are critical to determine the probability that a conformal TMD shell will form on the core. The core morphology, along with TMD synthesis conditions discussed in the prior section, largely dictates the morphology of that TMD growth. The work discussed up until this point considers the case of a relatively smooth nanoparticle surface. However, evidence suggests that a rougher nanoparticle core can lead to flower-like growth, where multiple TMD sheets extend from the nanoparticle core. We show in Figure 5 that a large TiO₂ nanoparticle core that exhibits nanoscale crevices across the surface results in the flower-like TMD shell morphology. Flower-like TMD morphology is often observed and desired on TiO₂ nanoparticles because

additional TMD edge sites promote catalytic activity, but the reason for this morphology is not yet established.^{103,109} This effect has been attributed to the change in growth dynamics caused by the many crevices of anatase TiO₂, which serve as preferential nucleation sites for TMDs.¹⁰⁹ We hypothesize that this preferential binding at crevices leads to a variation in growth dynamics across the TiO₂ surface, which forces some layers to grow away from the TiO₂ core, similar to the discussion of winged core-shells above, and results in the flower-like morphology. Accordingly, TMD encapsulation of a rough nanoparticle provides a potential second pathway to achieve flower-like growth in Figure 5.

This discussion by no means provides an exhaustive list of all factors that impact the global structure of a TMD core-shell; however, these factors certainly can impact that structure, and we hope to present them as possible levers to manipulate core-shell morphology. Once a robust understanding of core-shell growth dynamics is established, a map of the complete parameter space of potential core-shell morphologies can be constructed.

V. Emerging opportunities

The next generation of curved TMDs will rely on templated substrates to enable nanoscale structure and property control. This review examines the use of nanoparticle cores as templates for curved TMDs, but a vast array of analysis and design opportunities await. Much remains unknown about the nanoscale structure and potential emergent properties of the TMD core-shell architecture. Building upon existing core-shell architectures and equipped with theoretical calculations, we aim to now expand and deepen the understanding of this catalog by suggesting future research directions to achieve new, particularly potent architectures for energy, optoelectronics, and quantum applications. A suite of diverse characterization methods has enabled the progress in and understanding of curved TMDs thus far. Microscopy, particularly electron microscopy, has begun to elucidate the detailed atomic and electronic-scale structure of TMD core-shells. Quantitative compositional techniques, such as energy dispersive x-ray spectroscopy (EDS) and x-ray photoelectron spectroscopy (XPS), are invaluable for investigating the

chemistry and interaction between core and shell. Similarly, global optical measurements, including photoluminescence, Raman, and UV-visible spectroscopies, are critical to probe emission and absorption changes in TMDs with varying core-shell structures. The next advent in this field – detecting and isolating emergent properties – will require highly sensitive characterization techniques with exceptional spatial resolution and precision. Among the aforementioned characterization techniques, transmission electron microscopy (TEM) and scanning transmission electron microscopy (STEM) and related techniques are particularly well suited to not only image structure but also to probe phenomena at the nano- and atomic-scale. Beyond the widely employed traditional imaging modes (e.g. conventional TEM), we discuss new opportunities to quantitatively discern nanoscale features^{110–113} and phenomena^{114–116} in curved TMDs by leveraging the multimodality of S/TEM.

Defect Engineering

A particularly fruitful area for further research builds on the idea that topological defects are needed to achieve a curved structure from a hexagonal lattice and seeks to attain those through a variety of architectures. With a continued emphasis on improving synthetic control over TMD core-shells, a route exists to deterministically attain a discrete number of topological defects dictated by geometry. These extended topological defects include dislocations, disclinations, and electromagnetic vortices and typically exist at interfaces where crystalline or magnetoelectric continuity is broken.² Non-topological defects further make curved TMD architectures unique. Because the formation energies for some atomic defects, such as sulfur vacancies, are significantly smaller in the curved geometry than the planar, synthesis protocols can be modified or *ex situ* radiation processes utilized to preferentially induce specific defects for desired applications.

The presence of defects leads to significant property modulation in TMDs, and thus achieving nanoscale control of defects would be quite enabling. The catalytic activity of TMDs, for instance, depends greatly on the defect concentration.^{117–120} This property enhancement paired with the appreciable

catalytic activities of various metal nanoparticle cores^{121–123} makes design of TMD core-shells a promising strategy. Additionally, various defects offer exotic features. 5 | 7 dislocations that form at grain boundaries in MoS₂ have been predicted to form local, ferromagnetic nanowires, while 4 | 8 dislocations are predicted to locally act as antiferromagnetic semiconductors.¹²⁴ Further, coupling between excitons and various atomic defects in TMDs has led to observations of single photon emission.^{125–127} The potential to achieve greater quantitative control over defect concentrations through architecture while simultaneously enhancing emission through coupling with metallic and dielectric resonator cores makes this an exciting avenue for future research.

The achievable resolution and precision¹²⁸ of S/TEM has made it an indispensable tool to identify atomic and structural defects and related phenomena in TMDs. Direct visualization of topological and non-topological defects combined with structural analysis via alternative S/TEM techniques can be leveraged to provide critical insight into defects in curved TMDs. For instance, fluctuations in chemical environment,¹²⁹ phonon distribution,¹³⁰ and bandgap¹³¹ and plasmonic¹³² responses due to the presence of defects can be probed with great accuracy in STEM using high resolution electron energy loss spectroscopy (EELS) and EDS.¹³³ In addition, recently developed high-speed direct electron detectors (DED) enable massive improvements in detection efficiency and noise floors.¹³⁴ This development has allowed for static imaging of materials using low electron beam flux to avoid damaging various beam-sensitive 2D materials.¹¹⁴ Moreover, collection of the forward-scattered STEM probe at many probe positions (so-called 4D-STEM) is possible with the high-speed readout of DED (in the microsecond range). These scanning nanodiffraction methods provide a means to attain sub-Å spatial resolution while enhancing contrast for low atomic number atoms. Together, these advances make it possible to readily identify defects in TMD layers.^{116,128,135} Further, the development of computational algorithms for high-throughput assessment of defects has opened pathways to confidently identify and quantify defect concentrations and provide a more detailed understanding of the relationship between defects and

architecture in these core-shell systems.^{136–138} Finally, these approaches can be extended into 3D through electron tomography.^{139–142} Through this method, recent studies have detected nanoscale defects, such as atomic-scale ripples and local strain tensors, and atomic scale defects, such as dopants and vacancies in nanoparticle and two-dimensional material systems.^{140,143,144}

Strain Engineering

The strain intrinsic to curved TMDs offers yet another engineering pathway. Here, we propose some of the more exotic property manipulation opportunities in these structures, including tuning electronic structure landscapes to locally confine and spatially funnel excitons and charge carriers.¹⁴⁵ In particular, because of the impact of strain on the local electronic structure and dielectric character, photogenerated excitons can be spatially localized to regions with maximum strain, as has been demonstrated across hundreds of nanometers.^{28,32,146} Inducing a heavily strained region through strategic design of core systems could enable exciton funneling and result in spatially-trapped photoemission. This feature would open applications in areas such as directional emission and lasing. Moreover, strain has also been predicted to modify the levels of exciton-phonon coupling¹⁴⁷ and circular dichroism¹⁴⁸, which thereby provides a great deal of potential tunability of optical emission emanating from an homogeneously strained TMD shell region.

Strain fields and their slight atomic displacements can be directly measured using S/TEM approaches such as geometric phase analysis (GPA).^{149,150} GPA has been used to map strain fields in planar materials, including TMDs, and also non-planar nanoparticles.^{114,151,152} By applying this approach to TMD core-shell geometries, regions of significant strain can be rapidly identified with atomic-scale resolution. When combined with recent advances in detection of nano- and atomic-scale defects, the ability to quantify strain in TMD core-shells becomes particularly powerful. Robust defect identification and strain quantification would greatly advance the understanding of the relationships between defects – both

topological and non-topological – and strain and open the door for more sophisticated defect and strain engineering opportunities.

Electric Field Manipulation

Unexplored core and shell combinations present rich opportunities to manipulate local electromagnetic fields and exploit optical and electronic properties in the TMD shell. While plasmonic core materials (e.g. Au and Ag) have historically served as an interesting platform to achieve this, a particularly unexplored and fruitful class of potential core materials is emerging photonic materials. High-index dielectrics (e.g. Si, Ge, TiO₂) are of particular interest to improve and control light emission from emitting materials because they can confine and direct light at the nanoscale without the high Ohmic losses characteristic of plasmonic metals.¹⁵³ The resonant electric and magnetic optical responses of high-index dielectrics can be coupled with exciton resonances to induce unique effects in TMDs, such as directional emission and Purcell enhancement.^{154–156} The energy transfer between a high-index dielectric particle and emitter can be enhanced based on their interfacial area, making the core-shell geometry highly attractive over a planar arrangement.^{157,158} The core-shell geometry not only provides the advantage of intimate contact with a high-index dielectric particle, but also, TMD shells can contribute additional magnetic dipole moment resonances.¹⁵⁷ Resonance coupling between high-index dielectric particles and TMDs in the core-shell geometry has been examined via simulation but not yet reported experimentally.^{157,158} Significant opportunity exists to experimentally demonstrate and study high-index dielectric@TMD structures, which should be achievable based on the low interface formation energy for Si/MoS₂ shown in Figure 4.

The S/TEM method differential phase contrast (DPC) allows for identification of electric field components in nanoscale samples, including core-shell architectures. Intrinsic electrostatic and magnetostatic fields within the sample modify the phase component of the transmitted electrons. DPC provides a method to measure changes in electric fields that may arise when parameters such as core size

or spacing are varied.^{111,159,160} Moreover, methods such as STEM Cathodoluminescence (STEM-CL) and EELS can also assess electric field information and resultant optical properties from TMD core-shells by identifying the distribution of photons generated when a sample is irradiated with the electron beam.^{161,162} Researchers have used these techniques for diverse analyses including probing quantum emitters¹⁶³ and surface plasmon oscillations.^{164–166} Additionally, these methods can be configured to detect the polarization or directionality within an emission spectrum,¹⁶⁷ thereby making it attractive for probing directional emission. These complementary methods allow for both understanding the optical response from a single core-shell particle and mapping the electric field distribution due to interactions between neighboring core-shell particles.

Topological Properties

Finally, TMD core-shell architectures offer promising applications in quantum computing due to their combination of hybridization and curvature. Quantum computing technology relies on quantum bits (i.e. qubits) coherently interacting with each other to achieve a state of superposition.¹⁶⁸ However, attaining and maintaining the level of coherent interaction needed to solve highly complex problems is quite challenging. Decoherence can occur due to a variety of sources, including the environment and neighboring qubits. Topological qubits are based on materials whose properties and structure are defined by their geometry and are intrinsically less susceptible to decoherence mechanisms. In such cases, the quantum signals in these materials are protected by the material shape and symmetry, making TMD core-shells an interesting platform for constructing topological qubits.^{169–171}

One approach to construct topological qubits that has gained recent popularity involves leveraging the “proximity effect”, where a strong topological insulator is directly interfaced with a superconductor.^{172,173} This approach can generate topologically non-trivial energy states at the interface between the two materials. Such an interface can be readily created in core-shell architectures. For instance, by encapsulating a traditional superconductor (e.g. an aluminum nanoparticle) with a TMD shell

exhibiting exotic behavior, such as spin quantum insulator phases at low temperatures,^{174–176} there exists a route to attain encodable states for topological computing. Additionally, strain can also serve as a lever in TMD core-shells to induce local phase transformations and create non-trivial states as evidenced in the case of WTe_2 .^{174,177} As such, by synthesizing TMDs on a curved platform and inducing an inhomogeneous strain profile, it is possible to attain local domains of non-topologically protected and topologically-protected states within a single layer.¹⁷⁸

Further, it is possible to manipulate the energy levels of quantum materials and populate particular states by breaking time-reversal symmetry in these core-shell architectures.¹⁷⁹ The heterostructure shell design detailed previously offers one potential route,⁵⁵ as a ferromagnetic or antiferromagnetic shell, such as nickel, vanadium, or iron dichalcogenides,^{180–182} can be synthesized on another atomically-thin shell. Additionally, gauge fields break time-reversal symmetry by inducing effects similar to a random magnetic field and have been predicted to arise in curved TMDs architectures due to topological defects.¹⁸³ While further experimental work is needed to confirm this prediction, time reversal symmetry breaking may be achievable with a wider variety of TMD layers as well.

Several advanced S/TEM techniques can be tailored to detect topological defects and features relevant for quantum applications in TMD core-shells. One such approach is Lorentz TEM, which provides information on the local magnetization at nanoscale interfaces.^{184,185} Further, it allows for real-time tracking of magnetic topological defects and spin textures, such as magnetic vortices and skyrmions, that might be induced in core-shell architectures.^{186–188} Additionally, electron holography, which induces wave function overlap between multiple electron beams,¹⁸⁹ is an excellent tool to study nanoscale quantum materials. This technique produces information about electrostatic and magnetostatic potentials within the sample.^{139,190–192} Electron holography can be directly extended from conventional planar architectures to TMD core-shells to detect similar interfacial phenomena while also mapping electrostatic interactions between individual nanoparticles.^{193,194} This tool can not only detect correlated states and phases but also

can elucidate how charge carriers respond to these perturbations, thereby providing a means to deduce tangible material properties such as local carrier concentrations and effective Fermi velocities.

Finally, these methods can be paired with EELS to acquire local electronic structure and magnetic property changes that can be used for information storage in quantum systems. Using momentum-resolved EELS techniques (q-EELS), it is possible to relate momentum and energy with nanoscale spatial resolution. Thus, this method can help determine electronic structure and identify local topological characteristics.^{195–197} For TMD core-shells, q-EELS can be used to map changes in electronic structure across interfacial regions, which can then be related to changes in magnetostatic or electrostatic properties. Similarly, magnetic structure from the sample can be attained via electron energy loss magnetic chiral dichroic spectra which detects changes in polarization caused by internal magnetic fields.^{198–200} Moreover, these measurements can be conducted as a function of various external perturbations, such as electric field, magnetic field, and temperature, to map how the system behaves across a wide phase space.

VI. Summary & Conclusions

This review discusses the emerging area of TMD core-shell architectures within the broader context of curved TMDs. We propose a geometric framework based on both dimensionality and curvature to highlight the role of curved TMDs within possible TMD architectures. TMD core-shells have already demonstrated promise in applications including optoelectronics and sensing due to their powerful ability to hybridize disparate nanomaterials through an intimate interface. However, more exotic properties, some of which are inaccessible to planar TMDs, could be achieved through advanced structural understanding and control of the curved TMD shell. Much of the local and atomic-scale structure of TMD core-shells can be understood by considering topological defects and strain in hollow curved TMDs. We augment this discussion of prior work with original calculation results to elucidate the impact of strain on defect formation energy and observe that formation energies are consistently lower in curved than planar

geometries. We detail investigations into the nanoscale structure and growth mechanisms of TMD core-shells, where future efforts can explore new core-shell morphologies and expand our proposed product pathways diagram. Finally, as evidenced by the discussion of future possibilities, ample opportunity awaits in both fundamental exploration and application-focused design of TMD core-shells, but it will require close collaboration between experts in theory, synthesis, and characterization. Before these structures can be fully harnessed for applications, sophisticated characterization is needed to unravel the type, location, and extent of defects and strain. We hope this review inspires researchers to appreciate the elegance of the TMD core-shell architecture and pursue the nanoscale understanding and engineering needed to realize its full design potential.

Methods

Density Functional Theory Calculations

We performed density functional theory calculations within the generalized-gradient approximation (GGA).²⁰¹ The projector augmented wave pseudopotentials are applied as implemented in the VASP package.²⁰² Calculations for MoS₂ structures are performed with a dense k-point mesh corresponding to 4000 k-points per reciprocal atom. The plane-wave basis-set cutoff energy is set to 500 eV, and the convergence criterion with respect to self-consistent iterations assumes the residual forces are less than 0.03 eV/Å.

The formation energy of a defect X is defined as in reference ²⁰³:

$$E^f(X) = E_{total}(X) - E_{total}(\text{bulk}) + \Delta n_i \mu_i$$

A negative formation energy suggests favorable formation, while positive values are unfavorable. In the equation, E_{total}^X and E_{total}^{bulk} are the total energies of a supercell containing the defect X and of a supercell of the perfect bulk material, respectively; μ_i is the atomic chemical potential of species i (and is referenced to the standard state), and Δn_i denotes the number of atoms of species i that have been added ($\Delta n_i > 0$) or removed ($\Delta n_i < 0$) to form the defect. Details on the interface formation energy calculations can be found in reference ⁵⁶.

TMD Core-Shell Synthesis

The TiO₂ nanoparticles were synthesized following the process from reference ²⁰⁴. MoS₂ encapsulation was achieved following the previous encapsulation process defined in reference ⁵⁶.

Conflict of Interest

The authors have no conflicts of interest to declare.

Acknowledgements

This material is based upon work supported by the National Science Foundation (NSF) under Grant No. DMR-1929356. S.H. and C.W. acknowledge funding from the U.S. Department of Commerce, National Institute of Standards and Technology (Award No. 70NANB14H012), as part of the Center for Hierarchical Materials Design (ChiMaD). This work made use of the EPIC facility of Northwestern University's NUANCE Center, which has received support from the SHyNE Resource (NSF-ECCS 2025633), the IIN, and Northwestern's MRSEC program (NSF DMR-1720139). A.A.M. gratefully acknowledges support from the Ryan Fellowship and the IIN at Northwestern University. The authors thank Dr. Wenjie Zhou and Dr. Haixin Lin for providing TiO₂ nanoparticles and Dr. Xiaomi Zhang for TEM expertise.

References

- (1) Gupta, S.; Saxena, A. *The Role of Topology in Materials*; Springer International Publishing AG, 2018.
- (2) Gupta, S.; Saxena, A. A Topological Twist on Materials Science. *MRS Bull.* **2014**, *39*, 265–279.
- (3) Chen, O.; Zhao, J.; Chauhan, V. P.; Cui, J.; Wong, C.; Harris, D. K.; Wei, H.; Han, H. S.; Fukumura, D.; Jain, R. K.; *et al.* Compact High-Quality CdSe-CdS Core-Shell Nanocrystals with Narrow Emission Linewidths and Suppressed Blinking. *Nat. Mater.* **2013**, *12*, 445–451.
- (4) Iijima, S. Helical Microtubules of Graphitic Carbon. *Nature* **1991**, *354*, 56–58.
- (5) Kroto, H. W.; Heath, J. R.; O'Brien, S. C.; Curl, R. F.; Smalley, R. E. C₆₀: Buckminsterfullerene. *Nature* **1985**, *318*, 162–163.
- (6) Mårtensson, T.; Patrik T. Svensson, C.; A. Wacaser, B.; W. Larsson, M.; Seifert, W.; Deppert, K.; Gustafsson, A.; Reine Wallenberg, L.; Samuelson, L. Epitaxial III–V Nanowires on Silicon. *Nano Lett.* **2004**, *4*, 1987–1990.
- (7) Cataldo, F.; Graovac, A.; Ori, O. *The Mathematics and Topology of Fullerenes*; Springer, 2011.
- (8) Terrones, H.; Terrones, M. Curved Nanostructured Materials. *New J. Phys.* **2003**, *5*, 126.1-126.37.
- (9) Kharisov, B. I.; Kharissova, O. V. *Carbon Allotropes: Metal-Complex Chemistry, Properties and Applications*; Springer, 2019.
- (10) Bertolazzi, S.; Jacopo, B.; Andras, K. Stretching and Breaking of Ultrathin MoS₂. *ACS Nano* **2011**, *5*, 9703–9709.
- (11) Kozawa, D.; Liu, P.; Zeng, Y.; Koman, V. B.; Kuehne, M.; Strano, M. S. Highly Ordered Two-Dimensional MoS₂ Archimedean Scroll Bragg Reflectors as Chromatically Adaptive Fibers. *Nano Lett.* **2020**, *20*, 3067–3078.
- (12) Hwang, D. Y.; Choi, K. H.; Park, J. E.; Suh, D. H. Highly Thermal-Stable Paramagnetism by Rolling up MoS₂ Nanosheets. *Nanoscale* **2017**, *9*, 503–508.
- (13) Cui, X.; Kong, Z.; Gao, E.; Huang, D.; Hao, Y.; Shen, H.; Di, C.-A.; Xu, Z.; Zheng, J.; Zhu, D. Rolling up Transition Metal Dichalcogenide Nanoscrolls via One Drop of Ethanol. *Nat. Commun.* **2018**, *9*, 1301.
- (14) Kumar, P.; Viswanath, B. Effect of Sulfur Evaporation Rate on Screw Dislocation Driven Growth of MoS₂ with High Atomic Step Density. *Cryst. Growth Des.* **2016**, *16*, 7145–7154.
- (15) Zhang, L.; Liu, K.; Wong, A. B.; Kim, J.; Hong, X.; Liu, C.; Cao, T.; Louie, S. G.; Wang, F.; Yang, P. Three-Dimensional Spirals of Atomic Layered MoS₂. *Nano Lett.* **2014**, *14*, 6418–6423.
- (16) Sarma, P. V.; Patil, P. D.; Barman, P. K.; Kini, R. N.; Shaijumon, M. M. Controllable Growth of Few-

- Layer Spiral WS₂. *RSC Adv.* **2016**, *6*, 376–382.
- (17) Ly, T. H.; Zhao, J.; Kim, H.; Han, G. H.; Nam, H.; Lee, Y. H. Vertically Conductive MoS₂ Spiral Pyramid. *Adv. Mater.* **2016**, *28*, 7723–7728.
- (18) Chen, X.; Yang, H.; Liu, G.; Gao, F.; Dai, M.; Hu, Y.; Chen, H.; Cao, W.; Hu, P.; Hu, W. Hollow Spherical Nanoshell Arrays of 2D Layered Semiconductor for High-Performance Photodetector Device. *Adv. Funct. Mater.* **2018**, *28*, 1705153.
- (19) Wu, J.; Nie, G.; Xu, J.; He, J.; Xu, Q.; Zhang, Z. Structural Instability and Mechanical Properties of MoS₂ Toroidal Nanostructures. *Phys. Chem. Chem. Phys.* **2015**, *17*, 32425–32435.
- (20) Cao, X.; Ding, C.; Zhang, C.; Gu, W.; Yan, Y.; Shi, X.; Xian, Y. Transition Metal Dichalcogenide Quantum Dots: Synthesis, Photoluminescence and Biological Applications. *J. Mater. Chem. B* **2018**, *6*, 8011–8036.
- (21) Kaplan-Ashiri, I.; Tenne, R. On the Mechanical Properties of WS₂ and MoS₂ Nanotubes and Fullerene-Like Nanoparticles: In Situ Electron Microscopy Measurements. *J. Miner. Met. Mater. Soc.* **2016**, *68*, 151–166.
- (22) Enyashin, A.; Gemming, S.; Seifert, G. Nanosized Allotropes of Molybdenum Disulfide. *Eur. Phys. J. Spec. Top.* **2007**, *149*, 103–125.
- (23) Bar-Sadan, M.; N. Enyashin, A.; Gemming, S.; Popovitz-Biro, R.; Y. Hong, S.; Prior, Y.; Tenne, R.; Seifert, G. Structure and Stability of Molybdenum Sulfide Fullerenes. *J. Phys. Chem. B* **2006**, *110*, 25399–25410.
- (24) Parilla, P. A.; Dillon, A. C.; Jones, K. M.; Riker, G.; Schulz, D. L.; Ginley, D. S.; Heben, M. J. The First True Inorganic Fullerenes? *Nature* **1999**, *397*, 114.
- (25) Tenne, R.; Seifert, G. Recent Progress in the Study of Inorganic Nanotubes and Fullerene-Like Structures. *Annu. Rev. Mater. Res.* **2009**, *39*, 387–413.
- (26) Bastide, S.; Duphil, D.; Borra, J.-P.; Lévy-Clément, C. WS₂ Closed Nanoboxes Synthesized by Spray Pyrolysis. *Adv. Mater.* **2006**, *18*, 106–109.
- (27) Hoshyargar, F.; Mugnaioli, E.; Branscheid, R.; Kolb, U.; Panthöfer, M.; Tremel, W. Structure Analysis on the Nanoscale: Closed WS₂ Nanoboxes through a Cascade of Topo- and Epitactic Processes. *CrystEngComm* **2014**, *16*, 5087–5092.
- (28) Castellanos-Gomez, A.; Rolda, R.; Cappelluti, E.; Buscema, M.; Guinea, F.; van der Zant, H. S. J.; Steele, G. A. Local Strain Engineering in Atomically Thin MoS₂. *Nano Lett.* **2013**, *13*, 5361–5366.
- (29) Conley, H. J.; Wang, B.; Ziegler, J. I.; Haglund, R. F.; Pantelides, S. T.; Bolotin, K. I. Bandgap Engineering of Strained Monolayer and Bilayer MoS₂. *Nano Lett.* **2013**, *13*, 3626–3630.
- (30) Iff, O.; Tedeschi, D.; Martín-Sánchez, J.; Moczala-Dusanowska, M.; Tongay, S.; Yumigeta, K.; Taboada-Gutiérrez, J.; Savaresi, M.; Rastelli, A.; Alonso-González, P.; *et al.* Strain-Tunable Single Photon Sources in WSe₂ Monolayers. *Nano Lett.* **2019**, *19*, 6931–6936.

- (31) Branny, A.; Kumar, S.; Proux, R.; Gerardot, B. D. Deterministic Strain-Induced Arrays of Quantum Emitters in a Two-Dimensional Semiconductor. *Nat. Commun.* **2017**, *8*, 1–7.
- (32) Li, H.; Contryman, A. W.; Qian, X.; Ardakani, S. M.; Gong, Y.; Wang, X.; Weisse, J. M.; Lee, C. H.; Zhao, J.; Ajayan, P. M.; *et al.* Optoelectronic Crystal of Artificial Atoms in Strain-Textured Molybdenum Disulphide. *Nat. Commun.* **2015**, *6*, 7381.
- (33) Hyde, S.; Ninham, B. W.; Andersson, S.; Larsson, K.; Landh, T.; Blum, Z.; Lidin, S. The Mathematics of Curvature. In *The Role of Curvature in Condensed Matter: Physics, Chemistry and Biology*; Elsevier, 1997; pp. 1–42.
- (34) Sgouros, A. P.; Kalosakas, G.; Sigalas, M. M.; Papagelis, K. Exotic Carbon Nanostructures Obtained through Controllable Defect Engineering. *RSC Adv.* **2015**, *5*, 39930–39937.
- (35) Lv, R.; Cruz-Silva, E.; Terrones, M. Building Complex Hybrid Carbon Architectures by Covalent Interconnections: Graphene-Nanotube Hybrids and More. *ACS Nano* **2014**, *8*, 4061–4069.
- (36) Pokropivny, V. V.; Skorokhod, V. V. New Dimensionality Classifications of Nanostructures. *Phys. E Low-Dimensional Syst. Nanostructures* **2008**, *40*, 2521–2525.
- (37) Teo, B. K.; Sun, X. H. Classification and Representations of Low-Dimensional Nanomaterials: Terms and Symbols. *J. Clust. Sci.* **2007**, *18*, 346–357.
- (38) Terrones, H.; Terrones, M.; Lopez-Urias, F.; Rodriguez-Manzo, J. A.; Mackay, A. L. Shape and Complexity at the Atomic Scale: The Case of Layered Nanomaterials. *Phil. Trans. R. Soc. Lond. A* **2004**, *362*, 2039–2063.
- (39) Bowick, M. J.; Giomi, L. Two-Dimensional Matter: Order, Curvature and Defects. *Adv. Phys.* **2009**, *58*, 449–563.
- (40) Terrones, M.; Hsu, W. K.; Hare, J. P.; Kroto, H. W.; Terrones, H.; Walton, M. Graphitic Structures: From Planar to Spheres, Toroids and Helices. *Phil. Trans. R. Soc. Lond. A* **1996**, *354*, 2025–2054.
- (41) Parilla, P. A.; Dillon, A. C.; Parkinson, B. A.; Jones, K. M.; Alleman, J.; Riker, G.; Ginley, D. S.; Heben, M. J. Formation of Nanooctahedra in Molybdenum Disulfide and Molybdenum Diselenide Using Pulsed Laser Vaporization. *J. Phys. Chem. B* **2004**, *108*, 6197–6207.
- (42) Chuang, C.; Jin, B. Y. Systematics of High-Genus Fullerenes. *J. Chem. Inf. Model.* **2009**, *49*, 1664–1668.
- (43) Dimitrakakis, G. K.; Tylianakis, E.; Froudakis, G. E. Pillared Graphene: A New 3-D Network Nanostructure for Enhanced Hydrogen Storage. *Nano Lett.* **2008**, *8*, 3166–3170.
- (44) Braun, E.; Lee, Y.; Moosavi, S. M.; Barthel, S.; Mercado, R.; Baburin, I. A.; Proserpio, D. M.; Smit, B. Generating Carbon Schwarzites via Zeolite-Templating. *Proc. Natl. Acad. Sci.* **2018**, *115*, E8116–E8124.
- (45) Evarestov, R. A. Sulfides. In *Theoretical Modeling of Inorganic Nanostructures. NanoScience and Technology*; Springer Berlin Heidelberg, 2015; pp. 611–651.

- (46) Enyashin, A. N. Theoretical Studies of Inorganic Fullerenes and Fullerene-Like Nanoparticles. *Isr. J. Chem.* **2010**, *50*, 468–483.
- (47) Panchakarla, L. S.; Tenne, R. Inorganic Nanotubes and Fullerene-Like Nanoparticles at the Crossroad between Materials Science and Nanotechnology and Their Applications with Regard to Sustainability. In *Nanotechnology for Energy Sustainability*; Wiley-VCH Verlag GmbH & Co. KGaA: Weinheim, Germany, 2017; pp. 745–780.
- (48) Eremina, O. E.; Semenova, A. A.; Sergeeva, E. A.; Polyakov, A. Y.; Professor, A. Z.; Polyakov, A. Y.; Zak, A.; Tenne, R.; Goodilin, E. A.; Solntsev, K. A. Nanocomposites Based on Tubular and Onion Nanostructures of Molybdenum and Tungsten Disulfides: Inorganic Design, Functional Properties and Applications. *Russ. Chem. Rev* **2018**, *87*, 251.
- (49) Albu-Yaron, A.; Sinha, S. S.; Tenne, R. Nanotubes from Two-Dimensional Materials in Contemporary Energy Research: Historical and Perspective Outlook. *ACS Energy Lett.* **2020**, *5*, 1498–1511.
- (50) Višić, B.; Panchakarla, L. S.; Tenne, R.; Višić, B.; Panchakarla, L. S.; Tenne, R. Inorganic Nanotubes and Fullerene-like Nanoparticles at the Crossroads between Solid-State Chemistry and Nanotechnology. *J. Am. Chem. Soc.* **2017**, *139*, 12865–12878.
- (51) Kim, I.; Park, S. W.; Kim, D. W. Onion-like Crystalline WS₂ Nanoparticles Anchored on Graphene Sheets as High-Performance Anode Materials for Lithium-Ion Batteries. *Chem. Eng. J.* **2019**, *375*, 122033.
- (52) Afanasiev, P. Topotactic Synthesis of Size-Tuned MoS₂ Inorganic Fullerenes That Allows Revealing Particular Catalytic Properties of Curved Basal Planes. *Appl. Catal. B Environ.* **2018**, *227*, 44–53.
- (53) Chhetri, M.; Gupta, U.; Yadgarov, L.; Rosentsveig, R.; Tenne, R.; Rao, C. N. R. Effects of P- and n-Type Doping in Inorganic Fullerene MoS₂ on the Hydrogen Evolution Reaction. *ChemElectroChem* **2016**, *3*, 1937–1943.
- (54) Zhang, Y. J.; Ideue, T.; Onga, M.; Qin, F.; Suzuki, R.; Zak, A.; Tenne, R.; Smet, J. H.; Iwasa, Y. Enhanced Intrinsic Photovoltaic Effect in Tungsten Disulfide Nanotubes. *Nature* **2019**, *570*, 349–353.
- (55) DiStefano, J. G.; Murthy, A. A.; Lescott, C. J.; dos Reis, R.; Li, Y.; Dravid, V. P. Au@MoS₂@WS₂ Core–Shell Architectures: Combining Vapor Phase and Solution-Based Approaches. *J. Phys. Chem. C* **2020**, *124*, 2627–2633.
- (56) DiStefano, J. G.; Li, Y.; Jung, H. J.; Hao, S.; Murthy, A. A.; Zhang, X.; Wolverton, C.; Dravid, V. P. Nanoparticle@MoS₂ Core–Shell Architecture: Role of the Core Material. *Chem. Mater.* **2018**, *30*, 4675–4682.
- (57) Li, Y.; Cain, J. D.; Hanson, E. D.; Murthy, A. A.; Hao, S.; Shi, F.; Li, Q.; Wolverton, C.; Chen, X.; Dravid, V. P. Au@MoS₂ Core-Shell Heterostructures with Strong Light-Matter Interactions. *Nano Lett.* **2016**, *16*, 7696–7702.
- (58) Fei, X.; Liu, Z.; Hou, Y.; Li, Y.; Yang, G.; Su, C.; Wang, Z.; Zhong, H.; Zhuang, Z.; Guo, Z. Synthesis of

- Au NP@MoS₂ Quantum Dots Core@shell Nanocomposites for SERS Bio-Analysis and Label-Free Bio-Imaging. *Materials* **2017**, *10*, 1–11.
- (59) Li, Z.; Jiang, S.; Huo, Y.; Liu, M.; Yang, C.; Zhang, C.; Liu, X.; Sheng, Y.; Li, C.; Man, B. Controlled-Layer and Large-Area MoS₂ Films Encapsulated Au Nanoparticle Hybrids for SERS. *Opt. Express* **2016**, *24*, 26097–26108.
- (60) Li, Z.; Jiang, S.; Huo, Y.; Liu, A.; Zhang, C.; Yu, J.; Wang, M.; Li, C.; Lu, Z.; Man, B. 3D Hybrid Plasmonic Nanostructures with Dense Hot Spots Using Monolayer MoS₂ as Sub-Nanometer Spacer. *Adv. Mater. Interfaces* **2018**, *5*, 1800661.
- (61) Li, Y.; DiStefano, J. G.; Murthy, A. A.; Cain, J. D.; Hanson, E. D.; Li, Q.; Castro, F. C.; Chen, X.; Dravid, V. P. Superior Plasmonic Photodetectors Based on Au@MoS₂ Core-Shell Heterostructures. *ACS Nano* **2017**, *11*, 10321–10329.
- (62) Zhu, Y. Q.; Hsu, W. K.; Kroto, H. W.; Walton, D. R. M. Carbon Nanotube Template Promoted Growth of NbS₂ Nanotubes/Nanorods. *Chem. Commun.* **2001**, 2184–2185.
- (63) Whitby, R. L. D.; Hsu, W. K.; Fearon, P. K.; Billingham, N. C.; Maurin, I.; Kroto, H. W.; Walton, D. R. M.; Boothroyd, C. B.; Firth, S.; Clark, R. J. H.; *et al.* Multiwalled Carbon Nanotubes Coated with Tungsten Disulfide. *Chem. Mater.* **2002**, *14*, 2209–2217.
- (64) Wang, Y.; Ma, Z.; Chen, Y.; Zou, M.; Yousaf, M.; Yang, Y.; Yang, L.; Cao, A.; Han, R. P. S. Controlled Synthesis of Core–Shell Carbon@MoS₂ Nanotube Sponges as High-Performance Battery Electrodes. *Adv. Mater.* **2016**, *28*, 10175–10181.
- (65) Liu, C.; Bai, Y.; Zhao, Y.; Yao, H.; Pang, H. MoS₂/Graphene Composites: Fabrication and Electrochemical Energy Storage. *Energy Storage Mater.* **2020**, *33*, 470–502.
- (66) Li, N.; Liu, Z.; Gao, Q.; Li, X.; Wang, R.; Yan, X.; Li, Y. In Situ Synthesis of Concentric C@MoS₂ Core–Shell Nanospheres as Anode for Lithium Ion Battery. *J. Mater. Sci.* **2017**, *52*, 13183–13191.
- (67) Ma, H.; Du, S.; Tao, H.; Li, T.; Zhang, Y. Three-Dimensionally Integrated Carbon Tubes/MoS₂ with Reduced Graphene Oxide Foam as a Binder-Free Anode for Lithium Ion Battery. *J. Electroanal. Chem.* **2018**, *823*, 307–314.
- (68) Yousaf, M.; Wang, Y.; Chen, Y.; Wang, Z.; Firdous, A.; Ali, Z.; Mahmood, N.; Zou, R.; Guo, S.; Han, R. P. S. A 3D Trilayered CNT/MoSe₂/C Heterostructure with an Expanded MoSe₂ Interlayer Spacing for an Efficient Sodium Storage. *Adv. Energy Mater.* **2019**, *9*, 1900567.
- (69) Maiti, P. S.; Ganai, A. K.; Bar-Ziv, R.; Enyashin, A. N.; Houben, L.; Bar Sadan, M. Cu_{2-x}S–MoS₂ Nano-Octahedra at the Atomic Scale: Using a Template to Activate the Basal Plane of MoS₂ for Hydrogen Production. *Chem. Mater.* **2018**, *30*, 4489–4492.
- (70) Bar-Ziv, R.; Ranjan, P.; Lavie, A.; Jain, A.; Garai, S.; Bar Hen, A.; Popovitz-Biro, R.; Tenne, R.; Arenal, R.; Ramasubramaniam, A.; *et al.* Au–MoS₂ Hybrids as Hydrogen Evolution Electrocatalysts. *ACS Appl. Energy Mater.* **2019**, *2*, 6043–6050.
- (71) Maiti, P. S.; Ganai, A. K.; Bar-Ziv, R.; Enyashin, A. N.; Houben, L.; Bar Sadan, M. Cu_{2-x}S–MoS₂ Nano-

- Octahedra at the Atomic Scale: Using a Template To Activate the Basal Plane of MoS₂ for Hydrogen Production. *Chem. Mater.* **2018**, *30*, 4489–4492.
- (72) Li, Y.; Majewski, M.; Islam, S.; Hao, S.; Murthy, A.; DiStefano, J.; Hanson, E.; Xu, Y.; Wolverton, C.; Kanatzidis, M.; *et al.* Morphological Engineering of Winged Au@MoS₂ Heterostructures for Electrocatalytic Hydrogen Evolution. *Nano Lett.* **2018**, *18*, 7104–7110.
- (73) Wang, J.; Zhou, Q.; Lu, Z.; Wei, Z.; Zeng, W. Gas Sensing Performances and Mechanism at Atomic Level of Au-MoS₂ Microspheres. *Appl. Surf. Sci.* **2019**, *490*, 124–136.
- (74) Prakash, R.; Nirala, N. R. One Step Synthesis of AuNPs@MoS₂-QDs Composite as a Robust Peroxidase-Mimetic for Instant Unaided Eye Detection of Glucose in Serum, Saliva, and Tear. *Sensors Actuators B* **2018**, *263*, 109–119.
- (75) Maji, S. K.; Yu, S.; Chung, K.; Ramasamy, M. S. Synergistic Nanozymetic Activity of Hybrid Gold Bipyramid-Molybdenum Disulfide Core@Shell Nanostructures for Two-Photon Imaging and Anticancer Therapy. *ACS Appl. Mater. Interfaces* **2018**, *10*, 42068–42076.
- (76) Tenne, R.; Margulis, L.; Genut, M.; Hodes, G. Polyhedral and Cylindrical Structures of Tungsten Disulfide. *Nature* **1992**, *360*, 444–446.
- (77) Iijima, S.; Ichihashi, T.; Ando, Y. Pentagons, Heptagons and Negative Curvature in Graphite Microtubule Growth. *Nature* **1992**, *356*, 776–778.
- (78) Mackay, A. L.; Terrones, H. Diamond from Graphite. *Nature* **1991**, *352*, 762.
- (79) Margullis, L.; Salitra, G.; Tenne, R.; Tallanker, M. Nested Fullerene-Like Structures. *Nature* **1993**, *365*, 113–114.
- (80) Seifert, G.; Terrones, H.; Terrones, M.; Jungnickel, G.; Frauenheim, T. Structure and Electronic Properties of MoS₂ Nanotubes. *Phys. Rev. Lett.* **2000**, *85*, 146–149.
- (81) Sadan, M. B.; Houben, L.; Enyashin, A. N.; Seifert, G.; Tenne, R.; Louie, S. G. Atom by Atom: HRTEM Insights into Inorganic Nanotubes and Fullerene-like Structures. *Proc. Natl. Acad. Sci.* **2008**, *105*, 15643–15648.
- (82) Enyashin, A. N.; Gemming, S.; Bar-Sadan, M.; Popovitz-Biro, R.; Hong, S. Y.; Prior, Y.; Tenne, R.; Seifert, G. Structure and Stability of Molybdenum Sulfide Fullerenes. *Angew. Chemie Int. Ed.* **2007**, *46*, 623–627.
- (83) Tenne, R.; Homyonfer, M.; Feldman, Y. Nanoparticles of Layered Compounds with Hollow Cage Structures (Inorganic Fullerene-Like Structures). *Chem. Mater.* **1998**, *10*, 3225–3238.
- (84) Enyashin, A.; Seifert, G. Inorganic Fullerenes and Nanotubes. In *Handbook of Nanophysics: Nanotubes & Nanowires*; CRC Press LLC, 2010; pp. 1–21.
- (85) Pietsch, S.; Dollinger, A.; Strobel, C. H.; Park, E. J.; Ganteför, G.; Seo, H. O.; Kim, Y. D.; Idrobo, J. C.; Pennycook, S. J. The Quest for Inorganic Fullerenes. *J. Appl. Phys.* **2015**, *118*, 134302.

- (86) Lavie, A.; Yadgarov, L.; Houben, L.; Popovitz-Biro, R.; Shaul, T.-E.; Nagler, A.; Suchowski, H.; Tenne, R. Synthesis of Core – Shell Single-Layer MoS₂ Sheathing Gold Nanoparticles, AuNP@MoS₂. *Nanotechnology* **2017**, *28*, 24LT03.
- (87) Srolovitz, D. J.; Safran, S. A.; Homyonfer, M.; Tenne, R. Morphology of Nested Fullerenes. *Phys. Rev. Lett.* **1995**, *74*, 1779–1783.
- (88) Srolovitz, D. J.; Safran, S. A.; Tenne, R. Elastic Equilibrium of Curved Thin Films. *Phys. Rev. E* **1994**, *49*, 5260–5270.
- (89) Li, N.; Lee, G.; Jeong, Y. H.; Kim, K. S. Tailoring Electronic and Magnetic Properties of MoS₂ Nanotubes. *J. Phys. Chem. C* **2015**, *119*, 6405–6413.
- (90) Yang, Y.; Liu, Y.; Man, B.; Zhao, M.; Li, W. Tuning the Electronic and Magnetic Properties of MoS₂ Nanotubes with Vacancy Defects. *RSC Adv.* **2019**, *9*, 17203–17210.
- (91) Enyashin, A. N.; Ivanovskiĭ, A. L. Atomic Defects of the Walls and the Electronic Structure of Molybdenum Disulfide Nanotubes. *Semiconductors* **2007**, *41*, 81–86.
- (92) Lorenz, T.; Teich, D.; Joswig, J.-O.; Seifert, G. Theoretical Study of the Mechanical Behavior of Individual TiS₂ and MoS₂ Nanotubes. *J. Phys. Chem. C* **2012**, *116*, 11714–11721.
- (93) Xiong, Q. L.; Zhang, J.; Xiao, C.; Li, Z. H. Effects of Atomic Vacancies and Temperature on the Tensile Properties of Single-Walled MoS₂ Nanotubes. *Phys. Chem. Chem. Phys.* **2017**, *19*, 19948–19958.
- (94) Wang, K.; Poretzky, A. A.; Hu, Z.; Srijanto, B. R.; Li, X.; Gupta, N.; Yu, H.; Tian, M.; Mahjouri-Samani, M.; Gao, X.; *et al.* Strain Tolerance of Two-Dimensional Crystal Growth on Curved Surfaces. *Sci. Adv.* **2019**, *5*, 1–10.
- (95) Li, H.; Tsai, C.; Koh, A. L.; Cai, L.; Contryman, A. W.; Fragapane, A. H.; Zhao, J.; Han, H. S.; Manoharan, H. C.; Abild-Pedersen, F.; *et al.* Activating and Optimizing MoS₂ Basal Planes for Hydrogen Evolution through the Formation of Strained Sulphur Vacancies. *Nat. Mater.* **2016**, *15*, 48–53.
- (96) Tsai, C.; Li, H.; Park, S.; Park, J.; Han, H. S.; Nørskov, J. K.; Zheng, X.; Abild-Pedersen, F. Electrochemical Generation of Sulfur Vacancies in the Basal Plane of MoS₂ for Hydrogen Evolution. *Nat. Commun.* **2017**, *8*, 1–8.
- (97) Li, J.; Kang, J.; Cai, Q.; Hong, W.; Jian, C.; Liu, W.; Banerjee, K. Boosting Hydrogen Evolution Performance of MoS₂ by Band Structure Engineering. *Adv. Mater. Interfaces* **2017**, *4*, 1700303.
- (98) Yin, L.; Hai, X.; Chang, K.; Ichihara, F.; Ye, J. Synergetic Exfoliation and Lateral Size Engineering of MoS₂ for Enhanced Photocatalytic Hydrogen Generation. *Small* **2018**, *14*, 1704153.
- (99) Wu, C.; Zhang, J.; Tong, X.; Yu, P.; Xu, J.; Wu, J.; Wang, Z. M.; Lou, J.; Chueh, Y. A Critical Review on Enhancement of Photocatalytic Hydrogen Production by Molybdenum Disulfide: From Growth to Interfacial Activities. *Small* **2019**, *1900578*, 1–25.

- (100) Li, Y.; Hao, S.; DiStefano, J.; Murthy, A.; Hanson, E.; Xu, Y.; Wolverton, C.; Chen, X.; Dravid, V. Site-Specific Positioning and Patterning of MoS₂ Monolayers: The Role of Au Seeding. *ACS Nano* **2018**, *12*, 8970–8976.
- (101) Häkkinen, H. The Gold-Sulfur Interface at the Nanoscale. *Nat. Chem.* **2012**, *4*, 443–455.
- (102) Kong, D.; Wang, H.; Cha, J. J.; Pasta, M.; Koski, K. J.; Yao, J.; Cui, Y.; J. Cha, J.; Pasta, M.; J. Koski, K.; *et al.* Synthesis of MoS₂ and MoSe₂ Films with Vertically Aligned Layers. *Nano Lett.* **2013**, *13*, 1341–1347.
- (103) Liu, X.; Xing, Z.; Zhang, Y.; Li, Z.; Wu, X.; Tan, S.; Yu, X.; Zhu, Q.; Zhou, W. Fabrication of 3D Flower-like Black N-TiO_{2-x}@MoS₂ for Unprecedented-High Visible-Light-Driven Photocatalytic Performance. *Appl. Catal. B Environ.* **2017**, *201*, 119–127.
- (104) Zhu, T.; Shen, W.; Wang, X.; Song, Y. F.; Wang, W. Paramagnetic CoS₂@MoS₂ Core-Shell Composites Coated by Reduced Graphene Oxide as Broadband and Tunable High-Performance Microwave Absorbers. *Chem. Eng. J.* **2019**, *378*, 122159.
- (105) Li, H.; Wu, H.; Yuan, S.; Qian, H. Synthesis and Characterization of Vertically Standing MoS₂ Nanosheets. *Sci. Rep.* **2016**, *6*, 1–9.
- (106) Zheng, B.; Chen, Y.; Qi, F.; Wang, X.; Zhang, W.; Li, Y.; Li, X. 3D-Hierarchical MoSe₂ Nanoarchitecture as a Highly Efficient Electrocatalyst for Hydrogen Evolution. *2D Mater.* **2017**, *4*, 025092.
- (107) Yu, J. H.; Lee, H. R.; Hong, S. S.; Kong, D.; Lee, H.-W.; Wang, H.; Xiong, F.; Wang, S.; Cui, Y. Vertical Heterostructure of Two-Dimensional MoS₂ and WSe₂ with Vertically Aligned Layers. *Nano Lett* **2015**, *15*, 1031–1035.
- (108) Wang, H.; Kong, D.; Johannes, P.; Cha, J. J.; Zheng, G.; Yan, K.; Liu, N.; Cui, Y. MoSe₂ and WSe₂ Nanofilms with Vertically Aligned Molecular Layers on Curved and Rough Surfaces. *Nano Lett.* **2013**, *13*, 3426–3433.
- (109) Wang, C.; Lin, H.; Liu, Z.; Wu, J.; Xu, Z.; Zhang, C. Controlled Formation of TiO₂/MoS₂ Core-Shell Heterostructures with Enhanced Visible-Light Photocatalytic Activities. *Part. Part. Syst. Charact.* **2016**, *33*, 221–227.
- (110) Jiang, Y.; Chen, Z.; Han, Y.; Deb, P.; Gao, H.; Xie, S.; Purohit, P.; Tate, M. W.; Park, J.; Gruner, S. M.; *et al.* Electron Ptychography of 2D Materials to Deep Sub-Ångström Resolution. *Nature* **2018**, *559*, 343–349.
- (111) Fang, S.; Wen, Y.; Allen, C. S.; Ophus, C.; Han, G. G. D.; Kirkland, A. I.; Kaxiras, E.; Warner, J. H. Atomic Electrostatic Maps of 1D Channels in 2D Semiconductors Using 4D Scanning Transmission Electron Microscopy. *Nat. Commun.* **2019**, *10*, 1–9.
- (112) Xu, R.; Chen, C. C.; Wu, L.; Scott, M. C.; Theis, W.; Ophus, C.; Bartels, M.; Yang, Y.; Ramezani-Dakhel, H.; Sawaya, M. R.; *et al.* Three-Dimensional Coordinates of Individual Atoms in Materials Revealed by Electron Tomography. *Nat. Mater.* **2015**, *14*, 1099–1103.

- (113) Van Der Zande, A. M.; Huang, P. Y.; Chenet, D. A.; Berkelbach, T. C.; You, Y.; Lee, G.-H. H.; Heinz, T. F.; Reichman, D. R.; Muller, D. A.; Hone, J. C. Grains and Grain Boundaries in Highly Crystalline Monolayer Molybdenum Disulphide. *Nat. Mater.* **2013**, *12*, 554–561.
- (114) Murthy, A. A.; Stanev, T. K.; Dos Reis, R.; Hao, S.; Wolverton, C.; Stern, N. P.; Dravid, V. P. Direct Visualization of Electric-Field-Induced Structural Dynamics in Monolayer Transition Metal Dichalcogenides. *ACS Nano* **2020**, *14*, 1569–1576.
- (115) He, K.; Shokuhfar, T.; Shahbazian-Yassar, R. Imaging of Soft Materials Using in Situ Liquid-Cell Transmission Electron Microscopy. *J. Phys. Condens. Matter* **2019**, *31*, 103001.
- (116) Ryu, G. H.; Zhu, T.; Chen, J.; Sinha, S.; Shautsova, V.; Grossman, J. C.; Warner, J. H. Striated 2D Lattice with Sub-nm 1D Etch Channels by Controlled Thermally Induced Phase Transformations of PdSe₂. *Adv. Mater.* **2019**, *31*, 1904251.
- (117) Ouyang, Y.; Ling, C.; Chen, Q.; Wang, Z.; Shi, L.; Wang, J. Activating Inert Basal Planes of MoS₂ for Hydrogen Evolution Reaction through the Formation of Different Intrinsic Defects. *Chem. Mater.* **2016**, *28*, 4390–4396.
- (118) Wang, S.; Sawada, H.; Han, X.; Zhou, S.; Li, S.; Guo, Z. X.; Kirkland, A. I.; Warner, J. H. Preferential Pt Nanocluster Seeding at Grain Boundary Dislocations in Polycrystalline Monolayer MoS₂. *ACS Nano* **2018**, *12*, 5626–5636.
- (119) Li, G.; Zhang, D.; Qiao, Q.; Yu, Y.; Peterson, D.; Zafar, A.; Kumar, R.; Curtarolo, S.; Hunte, F.; Shannon, S.; *et al.* All the Catalytic Active Sites of MoS₂ for Hydrogen Evolution. *J. Am. Chem. Soc.* **2016**, *138*, 16632–16638.
- (120) Shu, H.; Zhou, D.; Li, F.; Cao, D.; Chen, X. Defect Engineering in MoSe₂ for the Hydrogen Evolution Reaction: From Point Defects to Edges. *ACS Appl. Mater. Interfaces* **2017**, *9*, 42688–42698.
- (121) Linic, S.; Aslam, U.; Boerigter, C.; Morabito, M. Photochemical Transformations on Plasmonic Metal Nanoparticles. *Nat. Mater.* **2015**, *14*, 567–576.
- (122) Linic, S.; Christopher, P.; Xin, H.; Marimuthu, A. Catalytic and Photocatalytic Transformations on Metal Nanoparticles with Targeted Geometric and Plasmonic Properties. *Acc. Chem. Res.* **2013**, *46*, 1890–1899.
- (123) Wang, P.; Huang, B.; Dai, Y.; Whangbo, M. H. Plasmonic Photocatalysts: Harvesting Visible Light with Noble Metal Nanoparticles. *Phys. Chem. Chem. Phys.* **2012**, *14*, 9813–9825.
- (124) Zhang, Z.; Zou, X.; Crespi, V. H.; Yakobson, B. I. Intrinsic Magnetism of Grain Boundaries in Two-Dimensional Metal Dichalcogenides. *ACS Nano* **2013**, *7*, 10475–10481.
- (125) Srivastava, A.; Sidler, M.; Allain, A. V.; Lembke, D. S.; Kis, A.; Imamoglu, A. Optically Active Quantum Dots in Monolayer WSe₂. *Nat. Nanotechnol.* **2015**, *10*, 491–496.
- (126) He, Y. M.; Clark, G.; Schaibley, J. R.; He, Y.; Chen, M. C.; Wei, Y. J.; Ding, X.; Zhang, Q.; Yao, W.; Xu, X.; *et al.* Single Quantum Emitters in Monolayer Semiconductors. *Nat. Nanotechnol.* **2015**, *10*, 497–502.

- (127) Koperski, M.; Nogajewski, K.; Arora, A.; Cherkez, V.; Mallet, P.; Veuillen, J. Y.; Marcus, J.; Kossacki, P.; Potemski, M. Single Photon Emitters in Exfoliated WSe₂ Structures. *Nat. Nanotechnol.* **2015**, *10*, 503–506.
- (128) Wen, Y.; Ophus, C.; Allen, C. S.; Fang, S.; Chen, J.; Kaxiras, E.; Kirkland, A. I.; Warner, J. H. Simultaneous Identification of Low and High Atomic Number Atoms in Monolayer 2D Materials Using 4D Scanning Transmission Electron Microscopy. *Nano Lett.* **2019**, *19*, 6482–6491.
- (129) Krivanek, O. L.; Chisholm, M. F.; Nicolosi, V.; Pennycook, T. J.; Corbin, G. J.; Dellby, N.; Murfitt, M. F.; Own, C. S.; Szilagy, Z. S.; Oxley, M. P.; *et al.* Atom-by-Atom Structural and Chemical Analysis by Annular Dark-Field Electron Microscopy. *Nature* **2010**, *464*, 571–574.
- (130) Hage, F. S.; Nicholls, R. J.; Yates, J. R.; Mcculloch, D. G.; Lovejoy, T. C.; Dellby, N.; Krivanek, O. L.; Refson, K.; Ramasse, Q. M. Nanoscale Momentum-Resolved Vibrational Spectroscopy. *Sci. Adv.* **2018**, *4*.
- (131) Tizei, L. H. G.; Lin, Y.; Mukai, M.; Sawada, H.; Lu, A.; Li, L. Exciton Mapping at Subwavelength Scales in Two-Dimensional Materials. *Phys. Rev. Lett.* **2015**, *107601*, 1–5.
- (132) Nerl, H. C.; Winther, K. T.; Hage, F. S.; Thygesen, K. S.; Houben, L.; Backes, C.; Coleman, J. N.; Ramasse, Q. M.; Nicolosi, V. Probing the Local Nature of Excitons and Plasmons in Few-Layer MoS₂. *npj 2D Mater. Appl.* **2017**, *1*, 1–9.
- (133) Hage, F. S.; Kepaptsoglou, D. M.; Ramasse, Q. M.; Allen, L. J. Phonon Spectroscopy at Atomic Resolution. *Phys. Rev. Lett.* **2019**, *122*, 016103.
- (134) Battaglia, M.; Contarato, D.; Denes, P.; Giubilato, P. Cluster Imaging with a Direct Detection CMOS Pixel Sensor in Transmission Electron Microscopy. *Nucl. Instruments Methods Phys. Res. Sect. A Accel. Spectrometers, Detect. Assoc. Equip.* **2009**, *608*, 363–365.
- (135) Ophus, C. Four-Dimensional Scanning Transmission Electron Microscopy (4D-STEM): From Scanning Nanodiffraction to Ptychography and Beyond. *Microsc. Microanal.* **2019**, *25*, 563–582.
- (136) Lee, C. H.; Khan, A.; Luo, D.; Santos, T. P.; Shi, C.; Janicek, B. E.; Kang, S.; Zhu, W.; Sobh, N. A.; Schleife, A.; *et al.* Deep Learning Enabled Strain Mapping of Single-Atom Defects in Two-Dimensional Transition Metal Dichalcogenides with Sub-Picometer Precision. *Nano Lett.* **2020**, *20*, 3369–3377.
- (137) Hong, S.; Nomura, K. I.; Krishnamoorthy, A.; Rajak, P.; Sheng, C.; Kalia, R. K.; Nakano, A.; Vashishta, P. Defect Healing in Layered Materials: A Machine Learning-Assisted Characterization of MoS₂ Crystal Phases. *J. Phys. Chem. Lett.* **2019**, *10*, 2739–2744.
- (138) Patra, T. K.; Zhang, F.; Schulman, D. S.; Chan, H.; Cherukara, M. J.; Terrones, M.; Das, S.; Narayanan, B.; Sankaranarayanan, S. K. R. S. Defect Dynamics in 2-D MoS₂ Probed by Using Machine Learning, Atomistic Simulations, and High-Resolution Microscopy. *ACS Nano* **2018**, *12*, 8006–8016.
- (139) Midgley, P. A.; Dunin-Borkowski, R. E. Electron Tomography and Holography in Materials Science. *Nat. Mater.* **2009**, *8*, 271–280.

- (140) Tian, X.; Kim, D. S.; Yang, S.; Ciccarino, C. J.; Gong, Y.; Yang, Y.; Yang, Y.; Duschatko, B.; Yuan, Y.; Ajayan, P. M.; *et al.* Correlating the Three-Dimensional Atomic Defects and Electronic Properties of Two-Dimensional Transition Metal Dichalcogenides. *Nat. Mater.* **2020**, *19*, 867–873.
- (141) Arslan, I.; Tong, J. R.; Midgley, P. A. Reducing the Missing Wedge: High-Resolution Dual Axis Tomography of Inorganic Materials. *Ultramicroscopy* **2006**, *106*, 994–1000.
- (142) Biskupek, J.; Leschner, J.; Walther, P.; Kaiser, U. Optimization of STEM Tomography Acquisition - A Comparison of Convergent Beam and Parallel Beam STEM Tomography. *Ultramicroscopy* **2010**, *110*, 1231–1237.
- (143) Haberkorn, G.; Thaler, P.; Knez, D.; Volk, A.; Hofer, F.; Ernst, W. E.; Kothleitner, G. Formation of Bimetallic Clusters in Superfluid Helium Nanodroplets Analysed by Atomic Resolution Electron Tomography. *Nat. Commun.* **2015**, *6*, 1–6.
- (144) Willhammar, T.; Sentosun, K.; Mourdikoudis, S.; Goris, B.; Kurttepel, M.; Bercx, M.; Lamoen, D.; Partoens, B.; Pastoriza-Santos, I.; Pe´rez-Juste, J.; *et al.* Structure and Vacancy Distribution in Copper Telluride Nanoparticles Influence Plasmonic Activity in the Near-Infrared. *Nat. Commun.* **2017**, *8*, 1–7.
- (145) Carmesin, C.; Lorke, M.; Florian, M.; Erben, D.; Schulz, A.; Wehling, T. O.; Jahnke, F. Quantum-Dot-Like States in Molybdenum Disulfide Nanostructures Due to the Interplay of Local Surface Wrinkling, Strain, and Dielectric Confinement. *Nano Lett.* **2019**, *19*, 3182–3186.
- (146) Kumar, A.; Ahluwalia, P. K. Mechanical Strain Dependent Electronic and Dielectric Properties of Two-Dimensional Honeycomb Structures of MoX₂ (X=S, Se, Te). *Phys. B Condens. Matter* **2013**, *419*, 66–75.
- (147) Niehues, I.; Schmidt, R.; Drüppel, M.; Marauhn, P.; Christiansen, D.; Selig, M.; Berghäuser, G.; Wigger, D.; Schneider, R.; Braasch, L.; *et al.* Strain Control of Exciton-Phonon Coupling in Atomically Thin Semiconductors. *Nano Lett.* **2018**, *18*, 1751–1757.
- (148) Feierabend, M.; Morlet, A.; Berghäuser, G.; Malic, E. Impact of Strain on the Optical Fingerprint of Monolayer Transition-Metal Dichalcogenides. *Phys. Rev. B* **2017**, *96*, 045425.
- (149) Hütch, M. J.; Snoeck, E.; Kilaas, R. Quantitative Measurement of Displacement and Strain Fields from HREM Micrographs. *Ultramicroscopy* **1998**, *74*, 131–146.
- (150) Zhu, Y.; Ophus, C.; Ciston, J.; Wang, H. Interface Lattice Displacement Measurement to 1 Pm by Geometric Phase Analysis on Aberration-Corrected HAADF STEM Images. *Acta Mater.* **2013**, *61*, 5646–5663.
- (151) Johnson, C. L.; Snoeck, E.; Ezcurdia, M.; Rodríguez-González, B.; Pastoriza-Santos, I.; Liz-Marzán, L. M.; Hütch, M. J. Effects of Elastic Anisotropy on Strain Distributions in Decahedral Gold Nanoparticles. *Nat. Mater.* **2008**, *7*, 120–124.
- (152) Wetterskog, E.; Tai, C. W.; Grins, J.; Bergström, L.; Salazar-Alvarez, G. Anomalous Magnetic Properties of Nanoparticles Arising from Defect Structures: Topotaxial Oxidation of Fe_{1-x}O|Fe_{3-δ}O₄ Core|shell Nanocubes to Single-Phase Particles. *ACS Nano* **2013**, *7*, 7132–7144.

- (153) Jahani, S.; Jacob, Z. All-Dielectric Metamaterials. *Nat. Nanotechnol.* **2016**, *11*, 23–36.
- (154) Zhang, X.; Choi, S.; Wang, D.; Naylor, C. H.; Johnson, A. T. C.; Cubukcu, E. Unidirectional Doubly Enhanced MoS₂ Emission via Photonic Fano Resonances. *Nano Lett.* **2017**, *17*, 6715–6720.
- (155) Cihan, A. F.; Curto, A. G.; Raza, S.; Kik, P. G.; Brongersma, M. L. Silicon Mie Resonators for Highly Directional Light Emission from Monolayer MoS₂. *Nat. Photonics* **2018**, *12*, 284–290.
- (156) Chen, H.; Nanz, S.; Abass, A.; Yan, J.; Gao, T.; Choi, D.-Y. Y.; Kivshar, Y. S.; Rockstuhl, C.; Neshev, D. N. Enhanced Directional Emission from Monolayer WSe₂ Integrated onto a Multiresonant Silicon-Based Photonic Structure. *ACS Photonics* **2017**, *4*, 3031–3038.
- (157) Wang, H.; Wen, J.; Wang, W.; Xu, N.; Liu, P.; Yan, J.; Chen, H.; Deng, S. Resonance Coupling in Heterostructures Composed of Silicon Nanosphere and Monolayer WS₂: A Magnetic-Dipole-Mediated Energy Transfer Process. *ACS Nano* **2019**, *13*, 1739–1750.
- (158) Lepeshov, S.; Wang, M.; Krasnok, A.; Kotov, O.; Zhang, T.; Liu, H.; Jiang, T.; Korgel, B.; Terrones, M.; Zheng, Y.; *et al.* Tunable Resonance Coupling in Single Si Nanoparticle-Monolayer WS₂ Structures. *ACS Appl. Mater. Interfaces* **2018**, *10*, 16690–16697.
- (159) Yadav, A. K.; Nguyen, K. X.; Hong, Z.; García-Fernández, P.; Aguado-Puente, P.; Nelson, C. T.; Das, S.; Prasad, B.; Kwon, D.; Cheema, S.; *et al.* Spatially Resolved Steady-State Negative Capacitance. *Nature* **2019**, *565*, 468–471.
- (160) Song, B.; Ding, Z.; Allen, C. S.; Sawada, H.; Zhang, F.; Pan, X.; Warner, J.; Kirkland, A. I.; Wang, P. Hollow Electron Ptychographic Diffractive Imaging. *Phys. Rev. Lett.* **2018**, *121*.
- (161) Rocca, M. Low-Energy EELS Investigation of Surface Electronic Excitations on Metals. *Surf. Sci. Rep.* **1995**, *22*, 1–71.
- (162) Kociak, M.; Zagonel, L. F. Cathodoluminescence in the Scanning Transmission Electron Microscope. *Ultramicroscopy* **2017**, *176*, 112–131.
- (163) Zagonel, L. F.; Mazzucco, S.; Tence, March, K.; Bernard, R.; Laslier, B.; Jacopin, G.; Tchernycheva, M.; Rigutti, L.; Julien, F. H.; *et al.* Nanometer Scale Spectral Imaging of Quantum Emitters in Nanowires and Its Correlation to Their Atomically Resolved Structure. *Nano Lett.* **2011**, *11*, 568–573.
- (164) Vesseur, E. J. R.; De Waele, R.; Kuttge, M.; Polman, A. Direct Observation of Plasmonic Modes in Au Nanowires Using High-Resolution Cathodoluminescence Spectroscopy. *Nano Lett.* **2007**, *7*, 2843–2846.
- (165) Nicoletti, O.; De La Peña, F.; Leary, R. K.; Holland, D. J.; Ducati, C.; Midgley, P. A. Three-Dimensional Imaging of Localized Surface Plasmon Resonances of Metal Nanoparticles. *Nature* **2013**, *502*, 80–84.
- (166) Guzzinati, G.; Béch e, A.; Lourenço-Martins, H.; Martin, J.; Kociak, M.; Verbeeck, J. Probing the Symmetry of the Potential of Localized Surface Plasmon Resonances with Phase-Shaped Electron Beams. *Nat. Commun.* **2017**, *8*, 1–8.

- (167) Gomez-Medina, R.; Yamamoto, N.; Nakano, M.; Garcia de Abajo, F. J. Mapping Plasmons in Nanoantennas via Cathodoluminescence. *New J. Phys* **2008**, *10*, 105009.
- (168) Nayak, C.; Simon, S. H.; Stern, A.; Freedman, M.; Das Sarma, S. Non-Abelian Anyons and Topological Quantum Computation. *Rev. Mod. Phys.* **2008**, *80*, 1083–1159.
- (169) Kitaev, A. Y. Fault-Tolerant Quantum Computation by Anyons. *Ann. Phys.* **2003**, *303*, 2–30.
- (170) Kitaev, A. Anyons in an Exactly Solved Model and Beyond. *Ann. Phys.* **2006**, *321*, 2–111.
- (171) Lee, S. R.; Sharma, P. A.; Lima-Sharma, A. L.; Pan, W.; Nenoﬀ, T. M. Topological Quantum Materials for Realizing Majorana Quasiparticles. *Chem. Mater.* **2019**, *31*, 26–51.
- (172) Stanescu, T. D.; Sau, J. D.; Lutchyn, R. M.; Das Sarma, S. Proximity Effect at the Superconductor-Topological Insulator Interface. *Phys. Rev. B - Condens. Matter Mater. Phys.* **2010**, *81*, 241310.
- (173) Fu, L.; Kane, C. L. Superconducting Proximity Effect and Majorana Fermions at the Surface of a Topological Insulator. *Phys. Rev. Lett.* **2008**, *100*, 096407.
- (174) Soluyanov, A. A.; Gresch, D.; Wang, Z.; Wu, Q.; Troyer, M.; Dai, X.; Bernevig, B. A. Type-II Weyl Semimetals. *Nature* **2015**, *527*, 495–498.
- (175) Fatemi, V.; Wu, S.; Cao, Y.; Bretheau, L.; Gibson, Q. D.; Watanabe, K.; Taniguchi, T.; Cava, R. J.; Jarillo-Herrero, P. Electrically Tunable Low-Density Superconductivity in a Monolayer Topological Insulator. *Science* **2018**, *362*, 926–929.
- (176) Qi, Y.; Naumov, P. G.; Ali, M. N.; Rajamathi, C. R.; Schnelle, W.; Barkalov, O.; Hanfland, M.; Wu, S. C.; Shekhar, C.; Sun, Y.; *et al.* Superconductivity in Weyl Semimetal Candidate MoTe_2 . *Nat. Commun.* **2016**, *7*, 1–7.
- (177) Wu, Y.; Mou, D.; Jo, N. H.; Sun, K.; Huang, L.; Bud'Ko, S. L.; Canfield, P. C.; Kaminski, A. Observation of Fermi Arcs in the Type-II Weyl Semimetal Candidate WTe_2 . *RAPID Commun. Phys. Rev. B* **2016**, *94*, 121113.
- (178) Ma, Y.; Kou, L.; Li, X.; Dai, Y.; Smith, S. C.; Heine, T. Quantum Spin Hall Effect and Topological Phase Transition in Two-Dimensional Square Transition-Metal Dichalcogenides. **2015**, *92*.
- (179) Ferreira, G. J.; Loss, D. Magnetically Defined Qubits on 3D Topological Insulators. *Phys. Rev. Lett.* **2013**, *111*, 106802.
- (180) Zhao, G. L.; Callaway, J.; Hayashibara, M. Electronic Structures of Iron and Cobalt Pyrites. *Phys. Rev. B* **1993**, *48*, 15781–15786.
- (181) Fuh, H. R.; Chang, C. R.; Wang, Y. K.; Evans, R. F. L.; Chantrell, R. W.; Jeng, H. T. Newtype Single-Layer Magnetic Semiconductor in Transition-Metal Dichalcogenides VX_2 ($X = \text{S, Se and Te}$). *Sci. Rep.* **2016**, *6*, 1–11.
- (182) Matsuura, M.; Endoh, Y.; Hiraka, H.; Yamada, K.; Mishchenko, S.; Nagaosa, N.; Solov'yev, V. Classical and Quantum Spin Dynamics in the FCC Antiferromagnet NiS_2 with Frustration. *Phys.*

- Rev. B - Condens. Matter Mater. Phys.* **2003**, *68*, 094409.
- (183) Ochoa, H.; Zarzuela, R.; Tserkovnyak, Y. Emergent Gauge Fields from Curvature in Single Layers of Transition-Metal Dichalcogenides. *Phys. Rev. Lett.* **2017**, *118*, 026801.
- (184) Pollard, S. D.; Huang, L.; Buchanan, K. S.; Arena, D. A.; Zhu, Y. Direct Dynamic Imaging of Non-Adiabatic Spin Torque Effects. *Nat. Commun.* **2012**, *3*, 1–7.
- (185) Phatak, C.; Petford-Long, A. K.; De Graef, M. Recent Advances in Lorentz Microscopy. *Curr. Opin. Solid State Mater. Sci.* **2016**, *20*, 107–114.
- (186) Yu, X. Z.; Kanazawa, N.; Zhang, W. Z.; Nagai, T.; Hara, T.; Kimoto, K.; Matsui, Y.; Onose, Y.; Tokura, Y. Skyrmion Flow near Room Temperature in an Ultralow Current Density. *Nat. Commun.* **2012**, *3*, 1–6.
- (187) Mochizuki, M.; Yu, X. Z.; Seki, S.; Kanazawa, N.; Koshibae, W.; Zang, J.; Mostovoy, M.; Tokura, Y.; Nagaosa, N. Thermally Driven Ratchet Motion of a Skyrmion Microcrystal and Topological Magnon Hall Effect. *Nat. Mater.* **2014**, *13*, 241–246.
- (188) Yu, X. Z.; Onose, Y.; Kanazawa, N.; Park, J. H.; Han, J. H.; Matsui, Y.; Nagaosa, N.; Tokura, Y. Real-Space Observation of a Two-Dimensional Skyrmion Crystal. *Nature* **2010**, *465*, 901–904.
- (189) Lichte, H.; Lehmann, M. Electron Holography---Basics and Applications. *Reports Prog. Phys.* **2008**, *71*, 016102.
- (190) Uchida, M.; Tonomura, A. Generation of Electron Beams Carrying Orbital Angular Momentum. *Nature* **2010**, *464*, 737–739.
- (191) Schofield, M. A.; Beleggia, M.; Zhu, Y.; Pozzi, G. Characterization of JEOL 2100F Lorentz-TEM for Low-Magnification Electron Holography and Magnetic Imaging. *Ultramicroscopy* **2008**, *108*, 625–634.
- (192) Gatel, C.; Bonilla, F. J.; Meffre, A.; Snoeck, E.; Warot-Fonrose, B.; Chaudret, B.; Lacroix, L. M.; Blon, T. Size-Specific Spin Configurations in Single Iron Nanomagnet: From Flower to Exotic Vortices. *Nano Lett.* **2015**, *15*, 6952–6957.
- (193) Kern, F.; Linck, M.; Wolf, D.; Alem, N.; Arora, H.; Gemming, S.; Erbe, A.; Zettl, A.; Büchner, B.; Lubk, A. Autocorrected Off-Axis Holography of 2D Materials. *arXiv:2006.13855* **2020**.
- (194) Yamamoto, K.; Hogg, C. R.; Yamamuro, S.; Hirayama, T.; Majetich, S. A. Dipolar Ferromagnetic Phase Transition in Fe₃O₄ Nanoparticle Arrays Observed by Lorentz Microscopy and Electron Holography. *Appl. Phys. Lett.* **2011**, *98*, 072509.
- (195) Leapman, R. D.; Sun, S. Cryo-Electron Energy Loss Spectroscopy: Observations on Vitrified Hydrated Specimens and Radiation Damage. *Ultramicroscopy* **1995**, *59*, 71–79.
- (196) Wang, Y. Y.; Zhang, F. C.; Dravid, V. P.; Ng, K. K.; Klein, M. V.; Schnatterly, S. E.; Miller, L. L. Momentum-Dependent Charge Transfer Excitations in Sr₂CuO₂Cl₂ - Angle Resolved Electron Energy Loss Spectroscopy. *Phys. Rev. Lett.* **1996**, *77*, 1809–1812.

- (197) Wang, Y. Y.; Dravid, V. P.; Bulut, N.; Han, P. D.; Klein, M. V.; Schnatterly, S. E.; Zhang, F. C. Momentum-Transfer-Resolved Electron Energy Loss Spectroscopy of BaBiO₃: Anisotropic Dispersion of Threshold Excitation and Optically Forbidden Transition. *Phys. Rev. Lett.* **1995**, *75*, 2546–2549.
- (198) Schattschneider, P.; Hébert, C.; Rubino, S.; Stöger-Pollach, M.; Rusz, J.; Novák, P. Magnetic Circular Dichroism in EELS: Towards 10 Nm Resolution. *Ultramicroscopy* **2008**, *108*, 433–438.
- (199) Schattschneider, P.; Rubino, S.; Hébert, C.; Rusz, J.; Kuneš, J.; Novák, P.; Carlino, E.; Fabrizioli, M.; Panaccione, G.; Rossi, G. Detection of Magnetic Circular Dichroism Using a Transmission Electron Microscope. *Nature* **2006**, *441*, 486–488.
- (200) Rubino, S.; Schattschneider, P.; Stöger-Pollach, M.; Hébert, C.; Rusz, J.; Calmels, L.; Warot-Fonrose, B.; Houdellier, F.; Serin, V.; Novak, P. Energy-Loss Magnetic Chiral Dichroism (EMCD): Magnetic Chiral Dichroism in the Electron Microscope. *J. Mater. Res* **2017**, *23*, 2582–2590.
- (201) Perdew, J. P.; Burke, K.; Ernzerhof, M. Generalized Gradient Approximation Made Simple. *Phys. Rev. Lett.* **1996**, *77*, 3865–3868.
- (202) Kresse, G.; Furthmüller, J. Efficient Iterative Schemes for Ab Initio Total-Energy Calculations Using a Plane-Wave Basis Set. *Phys. Rev. B - Condens. Matter Mater. Phys.* **1996**, *54*, 11169–11186.
- (203) Janotti, A.; Van De Walle, C. G. Native Point Defects in ZnO. *Phys. Rev. B - Condens. Matter Mater. Phys.* **2007**, *76*, 165202.
- (204) Jiang, X.; Herricks, T.; Xia, Y. Monodispersed Spherical Colloids of Titania: Synthesis, Characterization, and Crystallization. *Adv. Mater.* **2003**, *15*, 1205–1209.
- (205) Kang, P.; Kim, K. H.; Park, H. G.; Nam, S. W. Mechanically Reconfigurable Architected Graphene for Tunable Plasmonic Resonances. *Light Sci. Appl.* **2018**, *7*, 1–9.
- (206) Chuang, C.; Fan, Y. C.; Jin, B. Y. Systematics of Toroidal, Helically-Coiled Carbon Nanotubes, High-Genus Fullerenes, and Other Exotic Graphitic Materials. *Procedia Eng.* **2011**, *14*, 2373–2385.
- (207) Smotlacha, J. The Chiral Massive Fermions in the Graphitic Wormhole. *J. Phys. Conf. Ser* **2014**, *563*, 012027.
- (208) Baimova, J. A.; Liu, B.; Dmitriev, S. V.; Zhou, K. Mechanical Properties of Crumpled Graphene under Hydrostatic and Uniaxial Compression. *J. Phys. D. Appl. Phys.* **2015**, *48*, 095302.
- (209) Zhang, Z.; Chen, J.; Li, B. Negative Gaussian Curvature Induces Significant Suppression of Thermal Conduction in Carbon Crystals. *Nanoscale* **2017**, *9*, 14208–14214.

Figures

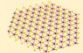









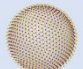
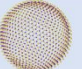
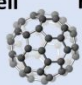
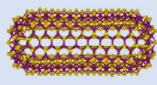

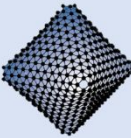
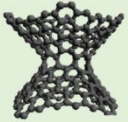

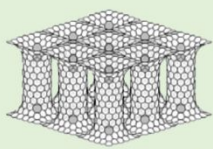
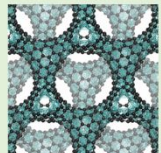
Architecture Dimensionality			
0D	1D	2D	3D
Zero Gaussian Curvature			
Planar			
 Quantum Dot	 Nanoribbon	 Monolayer	 Multilayer
Non-Planar			
 Nanoring	 Open Nanotube	 Wrinkled Sheet	 Crumpled Sheet
Mixed Curvature			
		 Torus	 Helicoidal Nanotube
Positive Gaussian Curvature			
 Core-shell	 Hollow Shell	 Fullerene	 Closed Nanotube
		Opportunity for development 	 Nanooctahedra
Negative Gaussian Curvature			
 Catenoid	Opportunity for development 	 Nanotube Network	 Schwartzite

Figure 1. Geometric framework for layered materials. Nanostructures based on TMDs and other layered materials are classified by both dimensionality and curvature. Dimensionality for each type of Gaussian curvature is defined based on the 0D structure (see text for full explanation) and thus varies between curvature types. The zero curvature category is divided into planar and non-planar structures, and the possibility that mixed (both positive and negative) curvature can arise from a zero curvature structure is demonstrated. This figure includes only those structures which have been either experimentally demonstrated or calculated for layered materials. Therefore, empty boxes represent areas particularly ripe for exploration where no structure fits a given dimensionality and curvature. Closed and helicoidal nanotubes reproduced by permission of IOP Publishing from ref. ⁸ © IOP Publishing & Deutsche Physikalische Gesellschaft. CC BY-NC-SA; Nanooctahedra reprinted by permission from Ref. ²⁴, Springer Nature: *Nature*, © 1999; Schwartzite reprinted from ref. ⁴⁴ under CC BY-NC-ND; Wrinkled sheet reproduced from ref. ²⁰⁵ under CC BY 4.0; Nanotube network reprinted from Ref. ²⁰⁶, © 2011 with

permission from Elsevier; Catenoid reprinted from ref. ²⁰⁷ under CC BY 3.0; Crumpled sheet reprinted from ref. ²⁰⁸ © IOP Publishing. Reproduced with permission. All rights reserved.

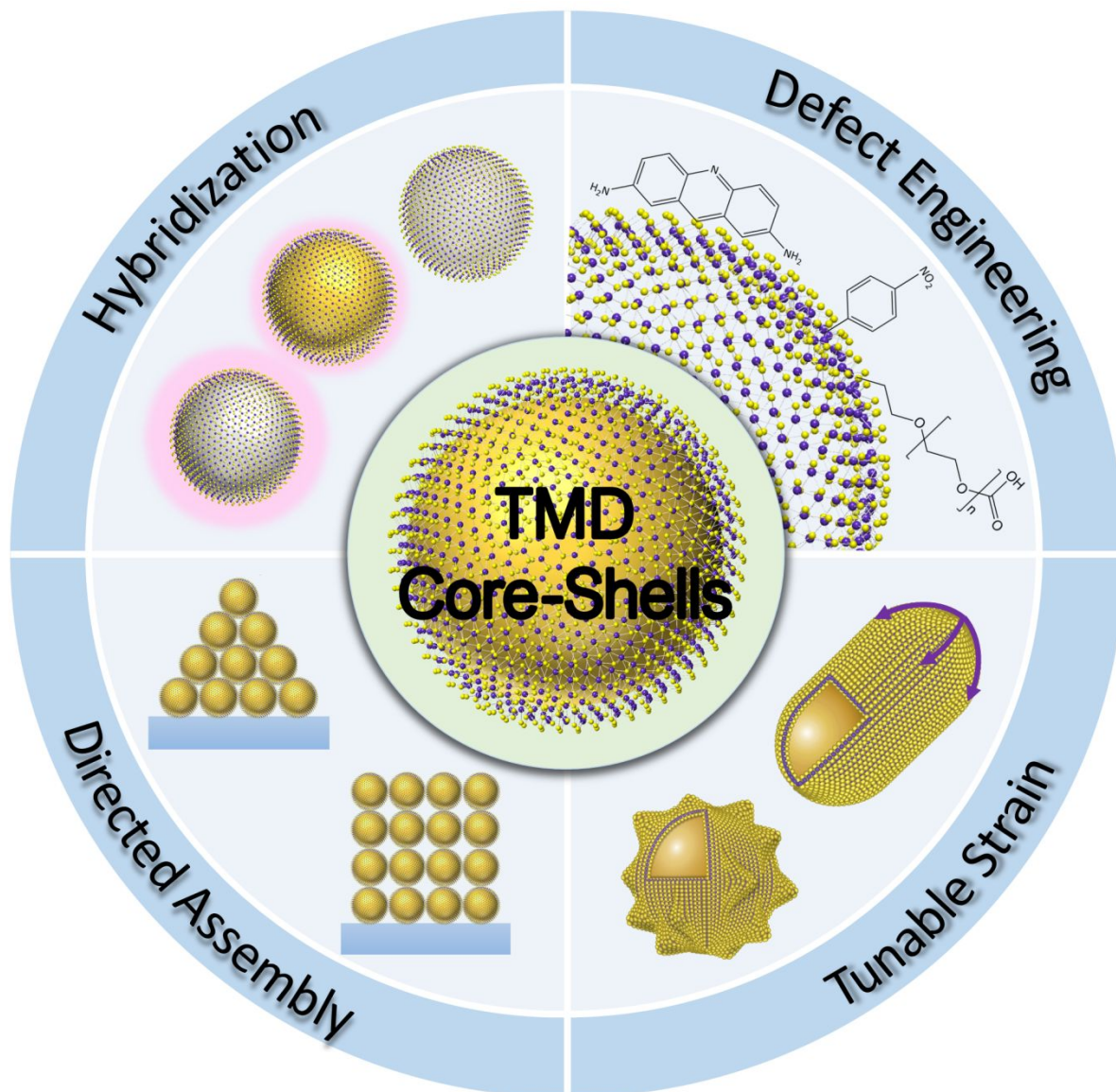


Figure 2. Functionality in TMD core-shells. TMD core-shells present several areas of added functionality compared to planar TMDs, including facile hybridization with other nanomaterials, defect engineering using topological or non-topological defects, strain engineering via controlled core shape, and direct assembly. Tunable strain structure models reprinted with permission from Ref. ⁷⁰ © 2019 American Chemical Society.

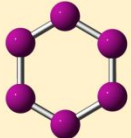
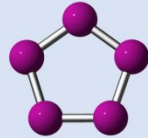
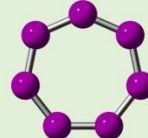
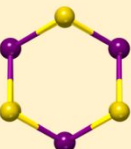
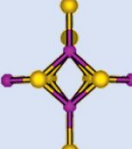
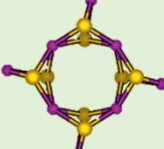
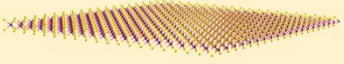
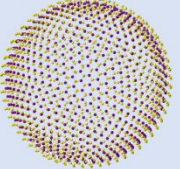
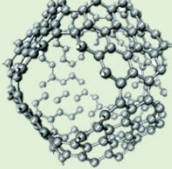
	Zero Gaussian Curvature	Positive Gaussian Curvature	Negative Gaussian Curvature
Topological Defect, Carbon	<p>Hexagon</p> 	<p>Pentagon</p> 	<p>Heptagon</p> 
Topological Defect, TMDs	<p>Hexagon</p> 	<p>Square-like defect</p> 	<p>Octagonal-like defect</p> 
Geometry			

Figure 3. Topological defects in layered materials. Defects are geometrically necessary to curve a hexagonal lattice; however, the type of defect varies based on the material chemistry. The top row demonstrates that pentagonal and heptagonal defects arise in curved carbon nanostructure to induce positive and negative curvature, respectively. The middle row demonstrates that TMDs instead exhibit square-like and octagonal-like defects in positive and negative curvature, respectively, due to the energy penalty of forming S-S or Mo-Mo bonds. It should be noted that curved carbon and TMD nanostructures will contain a combination of their respective topological defects and hexagonal rings. Examples of nanostructures exhibiting each type of curvature are shown in the bottom row. Square and octagonal defect models reprinted from ref. ⁸ © IOP Publishing & Deutsche Physikalische Gesellschaft. Reproduced by permission of IOP Publishing. CC BY-NC-SA; Negative curvature model reprinted from Ref. ²⁰⁹ with permission from the Royal Society of Chemistry.

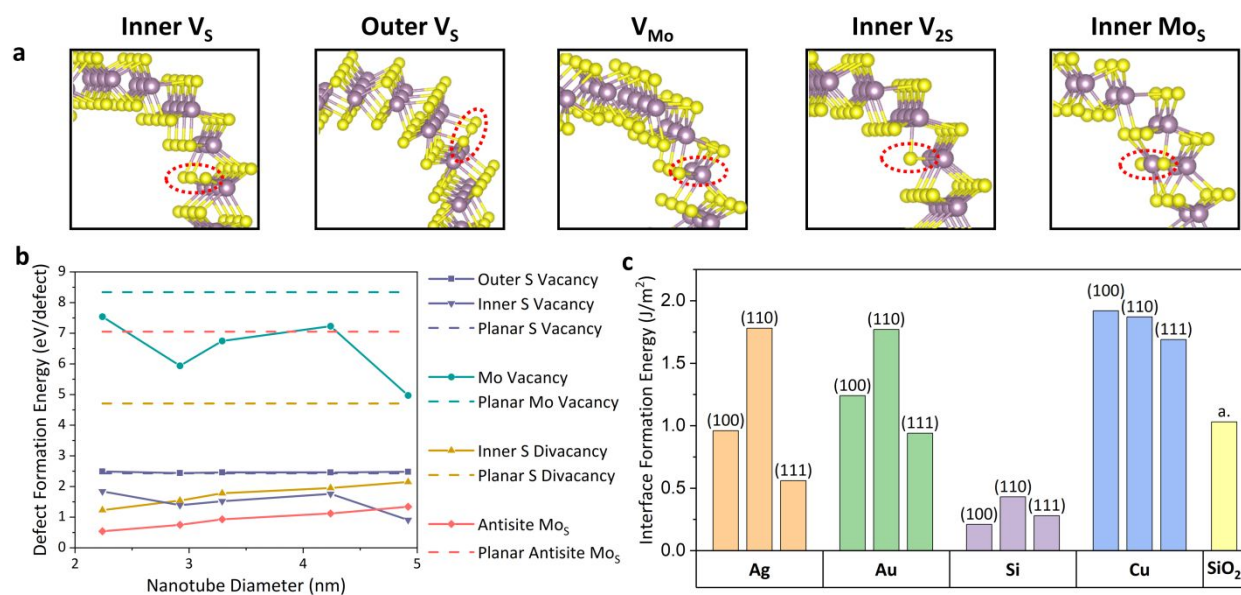


Figure 4. Density functional theory (DFT) calculations of defect and interface formation energies. (a) Atomic models demonstrating the calculated point defects in a single-layer MoS₂ nanotube. (b) DFT results for defect formation energy for each non-topological defect in MoS₂ nanotube and planar geometries. The defect formation energies in the nanotube are consistently lower than those in a planar sheet. (c) Interface formation energies, as calculated by DFT, for several potential core materials in TMD core-shells. The most favorable crystal faces of the core material are considered, where applicable, as these are the most likely faces to interface with a TMD shell. These calculations assumed a planar interface.

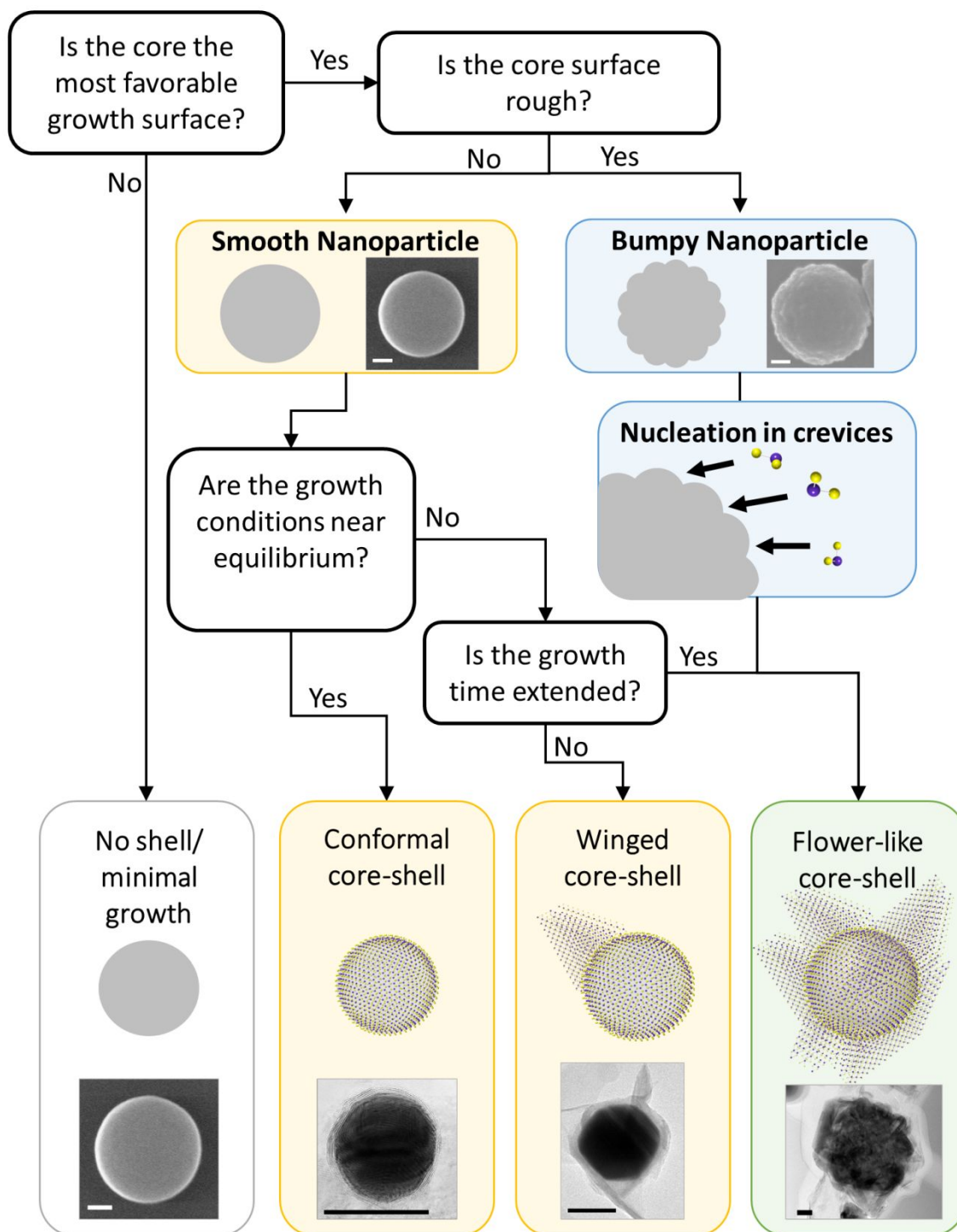


Figure 5. TMD core-shell product pathways. This figure demonstrates the various pathways that can produce four different core-shell products. The key factors represented are the core-shell interface formation energy, the roughness of the substrate, and the TMD synthesis conditions. The potential products range from no shell growth to a flower-like shell with many TMD sheets protruding from the core. All scale bars correspond to 50 nm. Images reprinted with permission from references ^{56,72} © 2018 American Chemical Society.

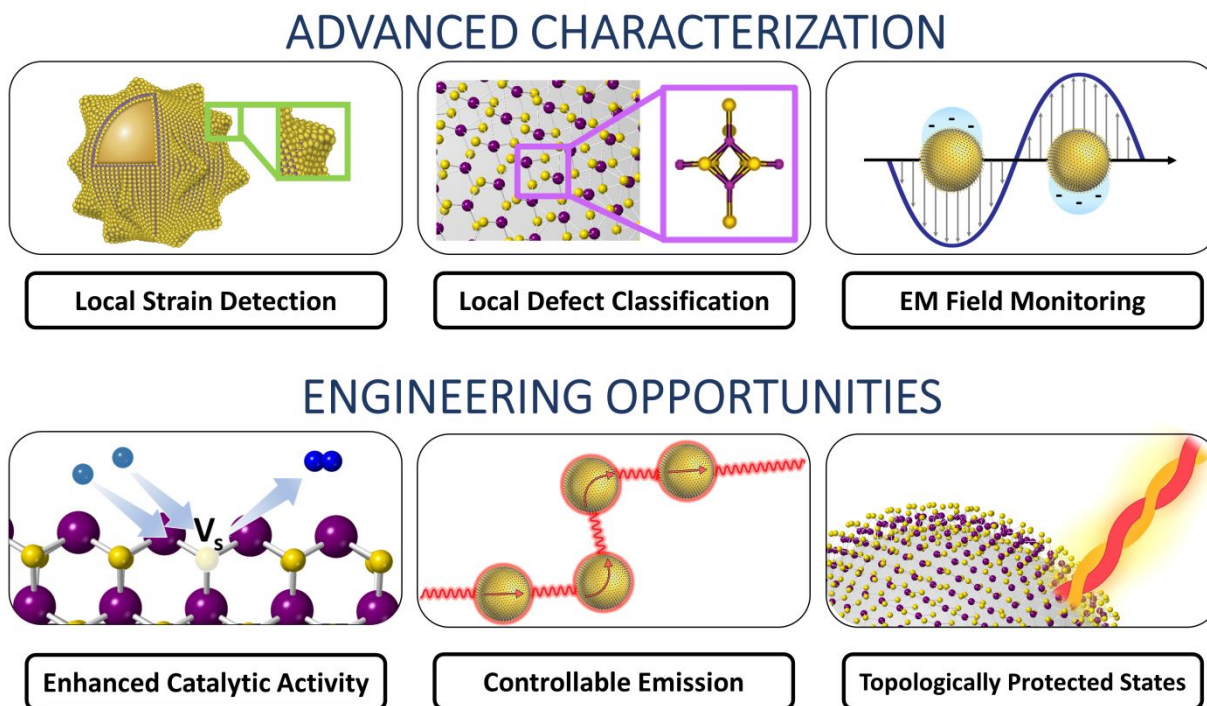


Figure 6. Emerging opportunities in TMD core-shells. Examples of some of the many future prospects for advanced characterization of TMD core-shells, including detection of local strain, defect classification, and understanding electric and magnetic fields. Potential engineering opportunities include enhancing catalytic activity, controlling optical emission, and attaining topologically protected states. Defect atomic model reprinted from Ref. ⁸ © IOP Publishing & Deutsche Physikalische Gesellschaft. Reproduced by permission of IOP Publishing. CC BY-NC-SA; Strained model reprinted with permission from Ref. ⁷⁰ © 2019 American Chemical Society.

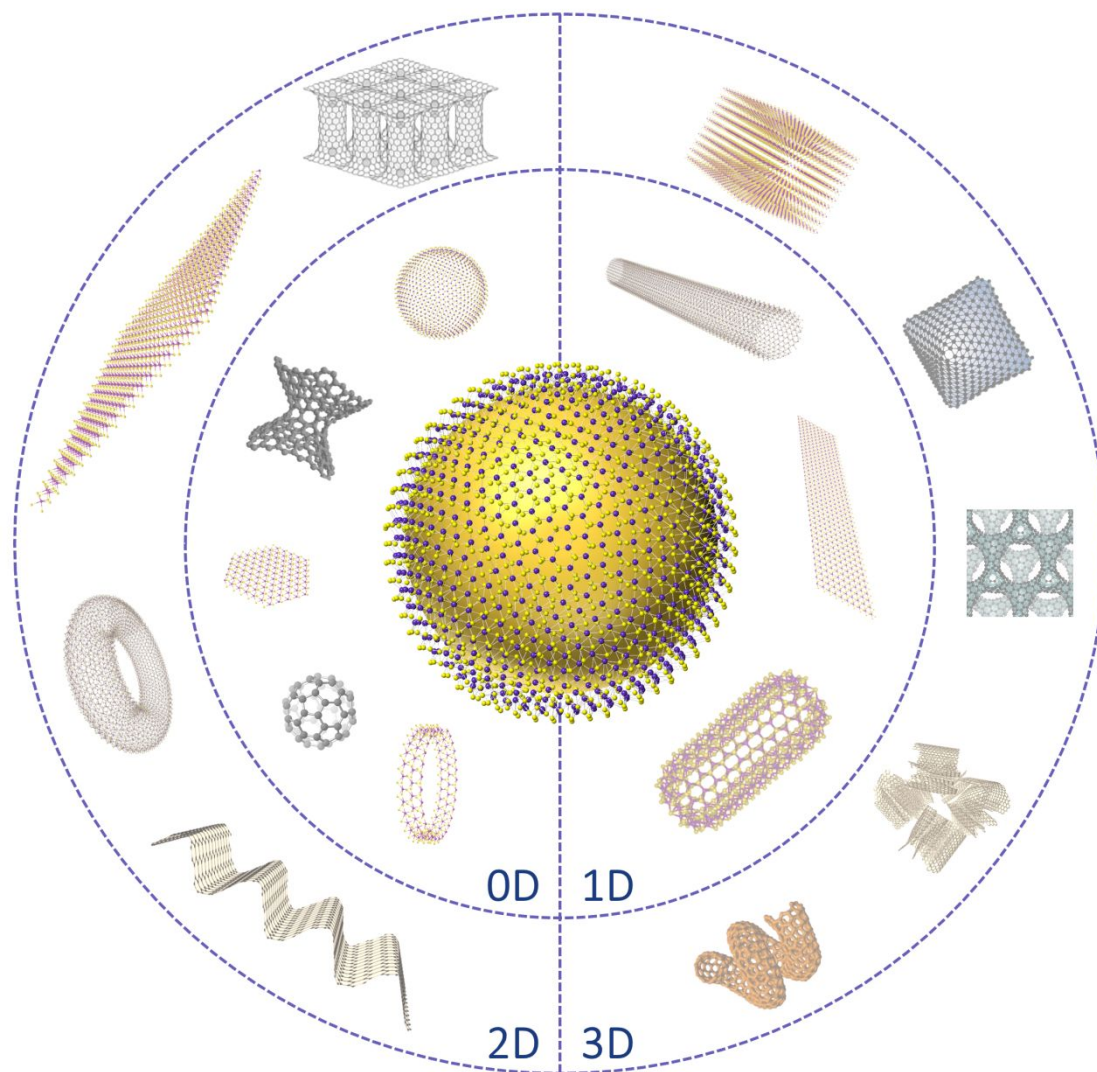


Table of Contents Figure.

Novelty statement: This review paper highlights the rich opportunities of curvature and architecture in transition metal dichalcogenides for improved material design.